



A Unified Formula for Small-Strain Shear Modulus of Sandy Soils Based on Extreme Void Ratios

Ke Liang¹; Guoxing Chen²; Xiuli Du³; Chengshun Xu⁴; and Jun Yang, F.ASCE⁵

Abstract: Small-strain shear modulus (G_0) is a fundamental property required in dynamic analyses. For sandy soils, G_0 may be affected strongly by particle characteristics such as uniformity coefficient (C_u), mean particle size (d_{50}), fines content (FC), and particle shape. Based on an extensive experimental study of the mechanical behavior of coral sands, this paper proposes a new formula for predicting G_0 for sandy soils with various C_u , d_{50} , FC, and particle shapes. A notable feature of the new formula is the use of the extreme void ratios (maximum void ratio e_{\max} and minimum void ratio e_{\min}) as the indexes, which were shown to be able to account for the effects of the various factors in a simple yet collective manner. Power-law correlations were established between the minimum small-strain shear modulus $G_{0\min}$ and e_{\max} as well as between the maximum small-strain shear modulus $G_{0\max}$ and e_{\min} . The wide applicability of this formula was validated further using extensive data from the literature from resonant column, bender element, and torsional shear tests on siliceous, calcareous, and coral sandy soils. DOI: 10.1061/JGGEFK.GTENG-10913. © 2022 American Society of Civil Engineers.

Author keywords: Sandy soil; Small-strain shear modulus; Particle characteristics; Extreme void ratio; Unified formula.

Introduction

The behavior of soils even at small strain levels exhibits nonlinearity. The shear modulus below strain levels of about 0.001% usually is termed the small strain shear modulus G_0 (Atkinson and Salfors 1991; Lo Presti 1995; Clayton and Heymann 2001; Clayton 2011). The G_0 and the strain-dependent shear modulus reduction G/G_0 and damping ratio λ curves are key information required in various geotechnical applications such as earthquake site response analysis and dynamic soil–structure interaction problems (e.g., Seed and Idriss 1970; Kokusho 1980; Rollins et al. 1998, 2020; Yang and Yan 2009; Senetakis et al. 2012, 2013; Yang and Gu 2013; Oztoprak and Bolton 2013; Chen et al. 2016; Senetakis and He 2017; Chen et al. 2019b, 2021c, 2022). Extensive research has measured the G_0 of sandy soils in laboratory measurements [cyclic triaxial (CTX) tests, resonant column (RC) tests, bender element (BE) tests, and so forth] and in situ shear wave velocity (V_s) measurements via the fundamental relation $G_0 = \rho V_s^2$, in which ρ is the soil mass density. The G_0 of sandy soils is governed by the soil

material properties {e.g., particle-size distribution features [uniformity coefficient C_u , mean particle size d_{50} , and fines content (FC)], particle shape, fabric, and mineralogy} and its state (e.g., global void ratio e or relative density D_r , mean effective confining stress σ'_c or vertical effective stress σ'_v) (e.g., Hardin and Richart 1963; Hardin and Black 1966; Seed and Idriss 1970; Seed et al. 1986; Rollins et al. 1998; Cubrinovski and Ishihara 2002; Menq 2003; Cho et al. 2006; Bui 2009; Wichtmann and Triantafyllidis 2009; Yilmaz and Mollamahmutoglu 2009; Clayton 2011; Senetakis et al. 2012, 2013; Gu et al. 2013; Altuhafi et al. 2016; Payan et al. 2016; Sarkar et al. 2019; Chen et al. 2019b, 2020). The influence of loading rate on the G_0 of a granular soil is negligible (Matesic and Vucetic 2003; Clayton 2011; Chen et al. 2019b). The uncertainty of in situ V_s tests can lead to significant misinterpretation in the top 30 m, in which the average bias (ratio of standard deviation to mean value) of in situ methods appears to be 4%–14% within each method and 2.5%–12.6% between methods (Darvasi 2021). Given the difficulty of undisturbed sampling and the sophistication of cyclic laboratory element tests, along with the fact that in situ measurements of V_s are costly and time consuming, many researchers have attempted to establish empirical equations to predict G_0 (or V_s) based on the material properties and the state of the soil.

It is well recognized that the physical state parameters e (or D_r) and σ'_c (or σ'_v) are two very important factors governing the G_0 of sandy soils. Hardin's equation is one of the most popular empirical formulas for predicting G_0 of sandy and gravelly soils (Hardin and Richart 1963; Hardin and Black 1966)

$$G_0 = AF(e) \left(\frac{\sigma'_c}{P_a} \right)^n \quad (1)$$

where P_a = reference stress, usually atmosphere pressure (i.e., 100 kPa); A = material constant linked to soil type; and n = stress power, which strongly depends on the material properties (Ishihara 1996; Qadimi and Coop 2007; Gu and Yang 2013; Yang and Liu 2016; Chen et al. 2019b), and generally is in the range 0.35–0.7, and a value of 0.5 commonly is used for siliceous sands (Bui 2009; Clayton 2011), in which parameters A and n are linked to the particle gradation of sandy soil via C_u and d_{50} (Hardin and

¹Postdoctoral Researcher, The Key Laboratory of Urban Security and Disaster Engineering of Ministry of Education, Beijing Univ. of Technology, Beijing 100124, China.

²Professor, Institute of Geotechnical Engineering, Nanjing Tech Univ., Nanjing 210009, China; Director, Civil Engineering and Earthquake Disaster Prevention Center of Jiangsu Province, Nanjing 210009, China (corresponding author). ORCID: <https://orcid.org/0000-0001-9185-7488>. Email: gxc6307@163.com

³Professor, The Key Laboratory of Urban Security and Disaster Engineering of Ministry of Education, Beijing Univ. of Technology, Beijing 100124, China.

⁴Professor, The Key Laboratory of Urban Security and Disaster Engineering of Ministry of Education, Beijing Univ. of Technology, Beijing 100124, China.

⁵Professor, Dept. of Civil Engineering, Univ. of Hong Kong, Hong Kong, China.

Note. This manuscript was submitted on March 26, 2022; approved on September 2, 2022; published online on November 22, 2022. Discussion period open until April 22, 2023; separate discussions must be submitted for individual papers. This paper is part of the *Journal of Geotechnical and Geoenvironmental Engineering*, © ASCE, ISSN 1090-0241.

Richart 1963; Iwasaki and Tatsuoka 1977; Menq 2003; Cho et al. 2006; Wichtmann and Triantafyllidis 2009; Senetakis et al. 2012; Chen et al. 2019b); and $F(e)$ is a function of e and is expressed in different forms as follows:

Hardin and Black (1966) form

$$F(e) = \frac{(a - e)^2}{1 + e} \quad (2)$$

Bellotti et al. (1996) and Menq (2003) form

$$F(e) = e^{-b} \quad (3)$$

where a is a constant that depends mainly on particle shape and size, where $a = 2.17$ for rounded particles and $a = 2.97$ for angular particles; and b is a fitting constant between 1.1 and 1.5, with a mean value of 1.3 (Altuhafi et al. 2016). Rahman et al. (2014) proposed a modified version of the G_0 equation by replacing e with the equivalent skeleton void ratio e^* in Hardin's equation. Of more interest is the proposal by Yang and Liu (2016) which characterizes G_0 using the state parameter ψ instead of e and thus allows for a unified quantification for both clean and silty sands in the framework of critical state soil mechanics (Yang et al. 2018).

Another generally accepted formula for G_0 is expressed as a function of D_r and σ'_c (Seed and Idriss 1970)

$$G_0 = A_D K_2 \left(\frac{\sigma'_c}{P_a} \right)^n \quad (4)$$

where $n = 0.5$; and A_D and K_2 are material constants. Seed et al. (1986) showed that $A_D = 218.8$ MPa, and K_2 is a coefficient dependent on D_r , ranging from 30 for loose sand to 75 for dense sand, but the K_2 values are quite scattered (Rollins et al. 1998); Wichtmann and Triantafyllidis (2009) showed that $A_D = 17,700$ MPa, $n = 0.48$, and K_2 is a function of D_r for sandy soils

$$K_2 = \frac{1 + D_r}{(17.3 - D_r)^2} \quad (5)$$

where D_r = decimal form. For convenience, the combination of Eqs. (4) and (5) with the A_D and n values proposed by Wichtmann and Triantafyllidis (2009) is referred to as the updated Seed's equation.

Many researchers have observed that the particle-size distribution characteristics (C_u , d_{50} , and FC) of a sand soil may have significant effects on G_0 . Menq (2003) found that G_0 increases with C_u and d_{50} because e is associated closely with C_u . However, some researchers found that G_0 decreases with C_u and the influence of d_{50} on G_0 can be ignored (Wichtmann and Triantafyllidis 2009; Senetakis et al. 2012; Yang and Gu 2013; Liu et al. 2016; Ha Giang et al. 2017; Gu et al. 2017). Wichtmann and Triantafyllidis (2009) stated that the proportion of contact force chains in nonuniformly composed material with larger C_u is smaller than those in the uniformly composed material with lower C_u , which results in the decrease of G_0 with the increase of C_u . Yang and Gu (2013) proposed a micromechanics-based explanation using the Hertz–Mindlin contact law, suggesting that G_0 is independent of particle size. Gu et al. (2017) showed that G_0 is independent of d_{50} and it decreases with increasing C_u at the same e and σ'_c . Moreover, several researchers have shown that an increase of FC (below a threshold fines content FC_{th}) may result in a decrease of G_0 , and the decreasing rate decreases as FC increases (e.g., Iwasaki and Tatsuoka 1977; Salgado et al. 2000; Wichtmann et al. 2015; Yang and Liu 2016; Shi et al. 2020). There may be interactions between the effects of C_u , d_{50} , and FC on the G_0 value of sandy soils (Chen et al. 2020). For a binary mixture, the FC_{th} is defined as

the fines content for distinguishing the regime of fines in sand from that of sand in fines. The G_0 value of the mixture may be quantified by the equivalent intergranular void ratio e^* (Thevanayagam et al. 2002; Chen et al. 2020; Rahmani and Naeini 2020).

In the literature, several modified G_0 equations have been proposed to consider the effects of C_u , d_{50} , and FC based on Hardin's equation (e.g., Menq 2003; Wichtmann and Triantafyllidis 2009; Payan et al. 2016; Ha Giang et al. 2017), and a more general form is

$$G_0 = [A_1(C_u)A_2(d_{50})A_3(FC)]e^{-[b_1(C_u)b_2(d_{50})b_3(FC)]} \times \left(\frac{\sigma'_c}{P_a} \right)^{[n_1(C_u)n_2(d_{50})n_3(FC)]} \quad (6)$$

This equation does not consider the coupled effects of the various parameters, and it ignores the effect of particle shape. Cho et al. (2006) found a profound dependency of parameters A and n in Hardin's equation on the particle shape. In recent years, there has been increasing interest in the effect of particle shape on the mechanical properties of sandy soils (e.g., Yang and Wei 2012; Payan et al. 2016; Ha Giang et al. 2017; Chen et al. 2019b), and a notable attempt to characterize the shape based on G_0 was made by Liu and Yang (2018). Payan et al. (2016) found that the influence of particle gradation and shape on parameters A and n in Hardin's equation are decoupled, and attempted to quantify the influence of particle shape on G_0 .

For sandy soils with different particle gradations and shapes, the extreme void ratios (maximum and minimum void ratios, denoted e_{max} and e_{min} , respectively) are used widely to describe the loosest and densest packing states, and they may reflect the inherent physical properties of these soils (Cubrinovski and Ishihara 1999, 2002; Cho et al. 2006; Sarkar et al. 2019). The packing structure of sandy soils is a fundamental factor governing the extreme void ratios (Youd 1973; Åberg 1992, 1996; Cubrinovski and Ishihara 2002; Menq 2003; Cho et al. 2006; Chang et al. 2017; Sarkar et al. 2019). Both e_{max} and e_{min} decrease significantly with the increase of C_u and regularity R (or sphericity s) (Cho et al. 2006; Altuhafi et al. 2016; Sarkar et al. 2019), but have no significant correlation with d_{50} (Youd 1973; Sarkar et al. 2019). In addition, both e_{max} and e_{min} significantly decrease with the increase of specific gravity G_s and can be expressed as a function of C_u , R , and G_s (Sarkar et al. 2019). The extreme void ratios first decrease and then increase with FC; the minimum values occur at FC = 20%–40%, and depends on the particle-size disparity ratio of the binary mixture (Cubrinovski and Ishihara 2002; Yilmaz and Mollamahmutoglu 2009; Chang et al. 2016; Chen et al. 2020). Several researchers have used ($e_{max} - e_{min}$) as an index to evaluate the liquefaction susceptibility of sandy and gravelly soils (Yilmaz and Mollamahmutoglu 2009; Chen et al. 2021a). Both e_{max} and e_{min} are intrinsic variables that reflect comprehensively the physical properties of granular soils. Thus, by introducing both e_{max} and e_{min} as indexes in the G_0 prediction equation, the various effects related to particle gradation, shape, and mineralogy can be captured properly. This was exactly the motivation of the present study.

Compared with siliceous sands, carbonate sediments with high content of calcium carbonate ($CaCO_3$) conventionally are referred to as calcareous sand. Carbonate sediments are divided into three categories: calcareous sand, with $CaCO_3 < 50\%$; siliceous carbonate sand, with $CaCO_3 = 50\%$ – 90% ; and carbonate sand, with $CaCO_3 \geq 90\%$ (Flores Lopez et al. 2018). Carbonate sand, which exists widely in coral reefs, mainly distributed in the area from 30° S to 30° N latitude, usually is called coral sand (Chen et al. 2021b, 2022; Ma et al. 2022). Coral sand particles have several obvious features, such as a rough surface, angular and irregular

shape, numerous intraparticle pores, low hardness, and fragileness (Sharma and Ismail 2006; Brandes 2011; Salem et al. 2013; Rui et al. 2020; Chen et al. 2021b, 2022; Cheng et al. 2022). There is no particle breakage in the first 1% shear strain during ring shearing of a coral sand under $\sigma'_v = 650\text{--}930\text{ kPa}$ (Coop et al. 2004). For the coral sand used in this study, the results of undrained cyclic triaxial tests showed that the values of the breakage index B in the Hardin (1985) method were less than 0.01 at $\sigma'_c = 300\text{ kPa}$ and $D_r = 76\%$ for axial strain (ε_a) levels up to 1% (Liang et al. 2020). Cheng et al. (2022) introduced a modified breakage index B based on the methods of Hardin (1985) and Einav (2007) and showed for a calcareous sand that the values of B are 0.013 at $D_r = 55\%$, $\sigma'_c = 300\text{ kPa}$, and $\varepsilon_a = 4\%$. Therefore, no significant particle breakage will occur for shear strains below 1% and σ'_c less than $\sim 300\text{ kPa}$ (i.e., the maximum values used in this study). Several studies have shown that significant differences in G_0 and in G/G_0 and λ over a range of strains exist between coral sands and siliceous sands (Ha Giang et al. 2017; Morsy et al. 2019; Liu et al. 2020; Rollins et al. 2020; Chen et al. 2022). Coral sand has a higher G_0 at the same e and σ'_c (Ha Giang et al. 2017), a larger n in Hardin's equation (Morsy et al. 2019), a higher G/G_0 at the same shear strain, and a lower λ for shear strains between 0.01% and 0.1% (Chen et al. 2022). However, little is known about the effects of C_u , d_{50} , FC, and particle morphology on the G_0 value of coral sands. In addition, Sandeep et al. (2021) found that the contact stiffness between two particles plays an important role in the stiffness–pressure relationship at very small to medium strains, which affects the stiffness of sands. In this respect, the roughness difference between coral sands and siliceous sands likely is a factor affecting the differences of G_0 , G/G_0 , and λ over a wide strain range.

Compared with laboratory tests (RC, BE, and CTX tests) and in situ V_s tests, index property tests are simpler, more rapid, more economical, and less uncertain (Chen et al. 2020). Thus it is desirable to characterize the G_0 value of sandy soils using the index properties. This paper presents results from a series of RC tests of coral sandy soils to investigate their G_0 values. The influence of various index properties (i.e. C_u , d_{50} , FC, e_{\max} , e_{\min} , and particle shape) was analyzed. A new extreme void ratios–based formula is proposed for predicting the G_0 of coral sandy soils. Furthermore, the applicability of this new formula was validated using data from the literature for various siliceous, calcareous, and coral sandy soils, covering a wide range of particle gradation and shape parameters.

Testing Apparatus, Materials, and Program

Testing Apparatus and Principle

A RC test apparatus (GCTS Instruments, Tempe, Arizona) was used in this research; it is a fixed-free type, i.e., the tested specimen is fixed on the pedestal and free to rotate at the top (Fig. 1). The details of the test apparatus were provided by Chen et al. (2019a). Uniform sinusoidal torsional excitations with constant amplitude are applied at the top of specimen over a wide frequency range via the cap of the RC apparatus by the motor-driven system. The data sampling system during the frequency sweeping can keep track of the shear strain amplitude (γ_a) value of the tested specimen. The theoretical background details of the RC test are provided by GCTS (2014) and Cataño-Arango (2006). The value of G_0 under the assumption of linear elastic material behavior is obtained from a frequency response curve associated with the variation in γ_a (Fig. 2). Thus, the resonant frequency (f_1) of the first rotational mode of the tested specimen can be measured using the sweeping

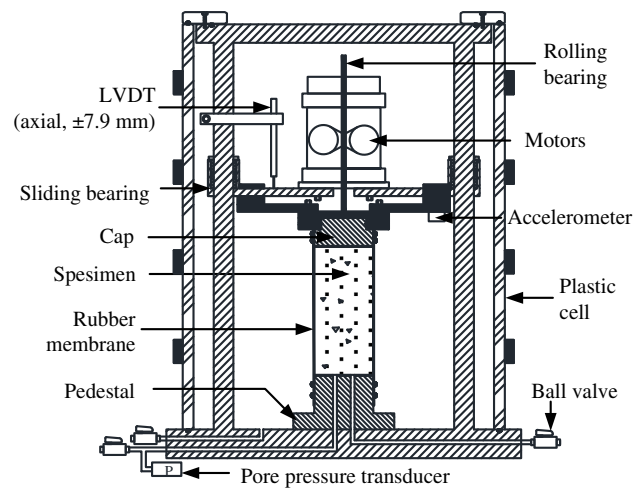


Fig. 1. Schematic of the resonant column test apparatus.

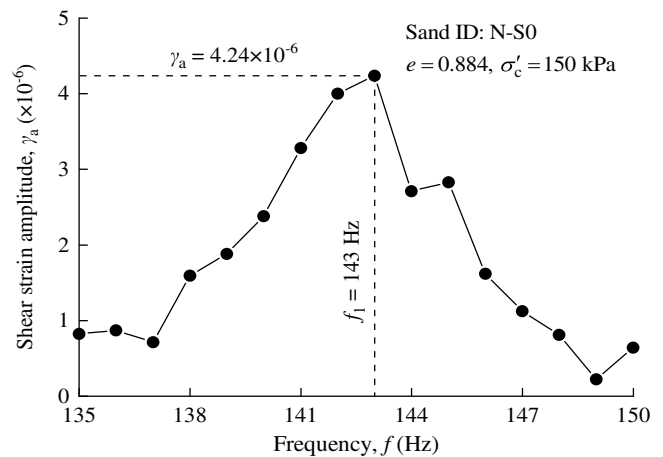


Fig. 2. Measured frequency responses of a specimen.

method. The V_s of the tested specimen can be determined using the measured f_1 . Via the relationship $G_0 = \rho V_s^2$, the following expression is obtained:

$$G = \rho \left(\frac{2\pi h f_1}{\beta} \right)^2 \quad (7)$$

where h = specimen height; and β = eigenvalue of vibration frequency equation, which is determined as follows:

$$\beta \tan(\beta) = I_s/I_t \quad (8)$$

where I_s = polar mass moment of inertia of tested specimen; I_t = polar mass moment of inertia of driving system; and $I_t = 8.80 \times 10^{-4}\text{ kg} \cdot \text{m}^2$ for the RC apparatus used herein.

Testing Material

The tested coral sandy soils were sampled from the coral reefs in the Nansha and Xisha Islands, South China Sea. Fig. 3 shows scanning electron microscope images of the Nansha and Xisha coral sand particles. The Nansha coral sand particles were composed of 55.5% aragonite, 41.5% high magnesian calcite, and 3.0%

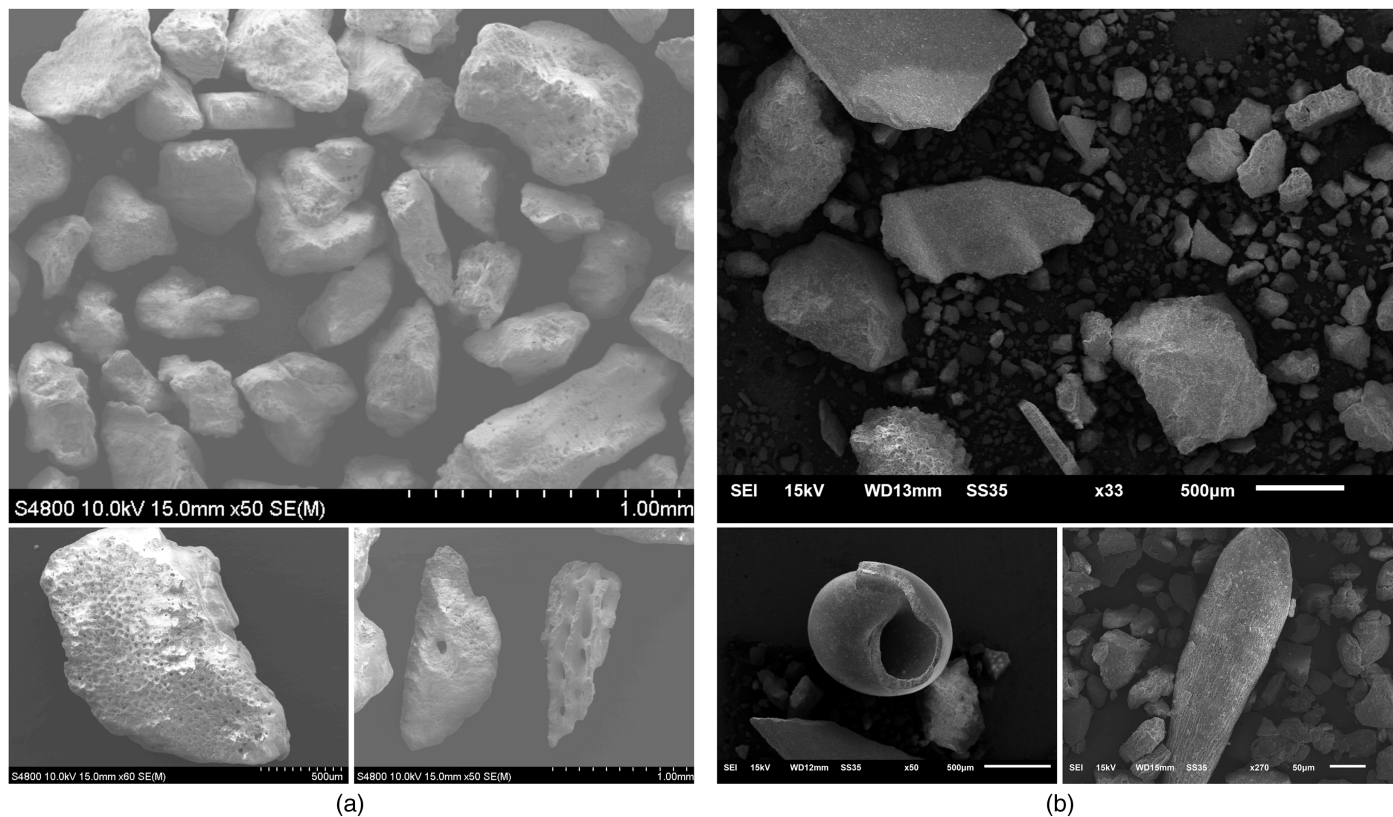


Fig. 3. Scanning electron microscope images of (a) Nansha coral sand particles; and (b) Xisha coral sand particles.

calcite, with specific gravity $G_s = 2.77$. The Nansha coral sand particles were coral debris with subangular to angular shapes, which had rough surfaces and numerous intraparticle pores. The particle sphericity s and roundness r , determined by visually comparing the shapes of ~ 30 particles with the characterization chart (Krumbein and Sloss 1963), were 0.31 and 0.57, respectively. Thus, the particle regularity $R = [(r + s)/2]$ was 0.44. The Xisha coral sand particles were composed of 78.3% aragonite, 19.3% high magnesian calcite, and 2.4% calcite, and contained a considerable proportion of shell debris besides the coral debris. The material properties were $G_s = 2.81$, $r = 0.19$, $s = 0.33$, and $R = 0.26$. As a result, the Xisha coral sand soils had more rod- and flake-shaped particles, and were more angular and irregular than the Nansha coral sand soils.

Nineteen coral sandy soils with various particle gradations, including 15 Nansha coral sandy soils and 4 Xisha coral sandy soils, were tested in this study. Clean coral sand with particle sizes ranging from 0.075 to 2 mm (Sand ID N-S0) and coral fines (< 0.075 mm) were sieved from the natural Nansha coral sandy soil. Fig. 4 shows the particle gradation curves of the 19 coral sandy soils and the pure coral fines, and Table 1 lists their index properties determined following the ASTM standards. The 19 sandy soils and the pure fines also were classified following the Unified Soil Classification System (ASTM 2011) (Table 1).

The e_{max} value was determined according to Method B of ASTM D4254 (ASTM 2016b). The material was pluviated from a funnel into a specific mold with zero dropping height to obtain the loosest packing to determine the value of e_{max} . The value of e_{min} was determined according to the improved procedure (Yamamuro and Lade 1997) for Vibration method 2A of ASTM D4253 (ASTM 2016a). To minimize segregation, the coral sandy soil was placed into the mold in 10 layers. Each layer was densified by static

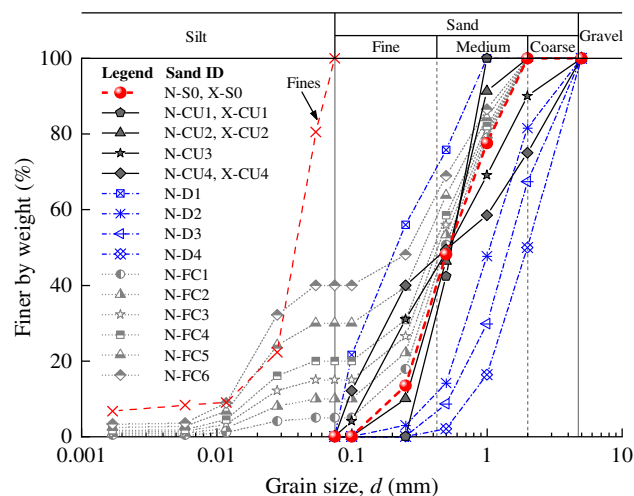


Fig. 4. Particle-size distribution curves of the tested coral sandy soils.

compaction at the layer surface and gently tapping the outside of the mold using a metal bar. The compaction was repeated until the volume of the soil no longer decreased and then the e_{min} value was determined. The e_{max} and e_{min} values of each coral sandy soil were tested several times until the relative errors were less than 2%. Fig. 5 shows e_{max} and e_{min} plotted versus C_u , d_{50} , and FC for the 19 coral sandy soils. The e_{max} and e_{min} values of the Xisha coral sandy soils were higher than those of the Nansha coral sandy soils, and both of them slightly decrease with C_u [Fig. 5(a)]. The influence of d_{50} and FC on the e_{max} and e_{min} values of the Nansha coral sandy soils were moderate or insignificant [Figs. 5(b and c)]. The e_{max} and

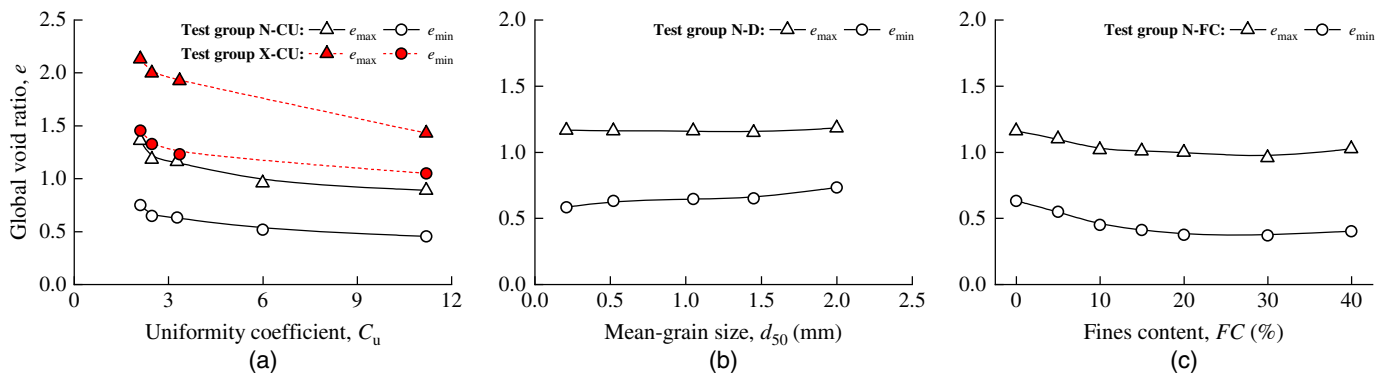
Table 1. Index properties of tested soils and best-fitted parameters in Hardin's equation

Sandy soil	Particle shape				Test group	Sand ID	Index properties ^a						Group symbol (USCS)	Eqs. (1) and (3)		
	G_s	r	s	R			C_u	C_c	d_{50} (mm)	FC (%)	e_{max}	e_{min}		A	b	n
Nansha coral sandy soil	2.77	0.31	0.57	0.44	N-CU	N-CU1	2.10	0.92	0.55	0	1.360	0.751	SP	90.52	1.15	0.47
						N-CU2	2.47	0.87	0.53	0	1.182	0.646	SP	76.43	1.17	0.50
						N-S0 ^b	3.35	0.93	0.52	0	1.162	0.631	SP	81.58	1.10	0.51
						N-CU3	5.99	0.65	0.52	0	0.958	0.516	SP	60.90	1.20	0.53
					N-D	N-CU4	11.20	0.32	0.52	0	0.890	0.453	SP	63.42	1.05	0.54
						N-D1	3.05	0.64	0.21	0	1.165	0.582	SP	67.25	1.15	0.51
						N-S0 ^b	3.35	0.93	0.52	0	1.162	0.631	SP	81.58	1.10	0.51
						N-D2	3.35	0.97	1.05	0	1.162	0.646	SP	80.65	1.11	0.50
					N-FC	N-D3	2.99	1.10	1.45	0	1.148	0.650	SP	80.77	1.14	0.50
						N-D4	3.26	0.99	2.00	0	1.183	0.733	SP	86.35	1.06	0.48
						N-S0 ^b	3.35	0.93	0.52	0	1.162	0.631	SP	81.58	1.10	0.51
						N-FC1	4.40	1.16	0.49	5	1.101	0.548	SP	65.26	1.16	0.51
						N-FC2	8.03	2.01	0.46	10	1.019	0.450	SW-SM	64.28	0.96	0.51
						N-FC3	24.46	5.76	0.43	15	1.009	0.412	SM	61.93	0.95	0.53
						N-FC4	29.25	5.86	0.40	20	0.999	0.375	SM	60.69	0.92	0.53
						N-FC5	32.29	0.88	0.34	30	0.958	0.369	SM	59.21	0.93	0.54
					—	N-FC6	30.22	0.15	0.27	40	1.025	0.401	SM	74.25	0.79	0.53
						Fines	3.41	1.73	0.038	100	—	—	ML	—	—	—
					Xisha coral sandy soil	2.81	0.19	0.33	0.26	X-CU	X-CU1	2.10	0.92	0.55	0	2.132
X-CU2	2.47	0.87	0.53	0							1.999	1.328	SP	157.87	1.77	0.51
X-S0	3.35	0.93	0.52	0							1.926	1.229	SP	137.07	1.61	0.53
X-CU4	11.20	0.32	0.52	0							1.430	1.050	SP	110.63	1.81	0.54

Note: USCS = Unified Soil Classification System.

^a $C_u = d_{60}/d_{10}$ and $C_c = d_{30}^2/(d_{10}d_{60})$, d_{10} , d_{30} , d_{50} , and d_{60} are particle sizes corresponding to 10%, 30%, 50%, and 60% finer on the cumulative particle-size distribution curve, respectively.

^bDuplicate sand in various test groups.

**Fig. 5.** Variations of e_{max} and e_{min} for the tested coral sandy soils in (a) Test groups N-CU and X-CU; (b) Test group N-D; and (c) Test group N-FC.

e_{min} values of the Nansha coral sandy soils reached their minimum values near $FC = 30\%$.

Specimen Preparation and Test Program

For RC tests, according to ASTM D3999/D3999M (ASTM 2013), three or four specimens of each coral sandy soil with various D_r values were prepared by a dry tamping (DT) method similar to the one used by Chen et al. (2021b). In this method, the oven-dried coral sand was placed in four sublayers into split molds from a funnel with near-zero falling head. Because the compaction of each succeeding layer would densify the previous sand layers, the layer masses were decreased slightly from top to bottom to obtain uniform density; thus the mass of each subsequent layer was 1%–2% less than that of the previous layer to obtain uniform density.

The specimens were 50 mm in diameter and 100 mm in height, and 63 specimens in total for the 19 coral sandy soils were tested in this study. Each specimen was consolidated isotropically in multiple stages to $\sigma'_c = 20$ (only for the Nansha coral sandy specimens), 50, 100, 150, 200, and 300 kPa. After each stage of consolidation, the axial deformation was measured and used to calculate the actual e value after consolidation based on an assumption of isotropic deformation. Thus, 366 data of G_0 were obtained in this study.

Test Results and Discussions

Fig. 6 plots G_0 versus e for the 19 coral sandy soils. The G_0 values of each coral sandy soil increased with σ'_c and decreased with e at a

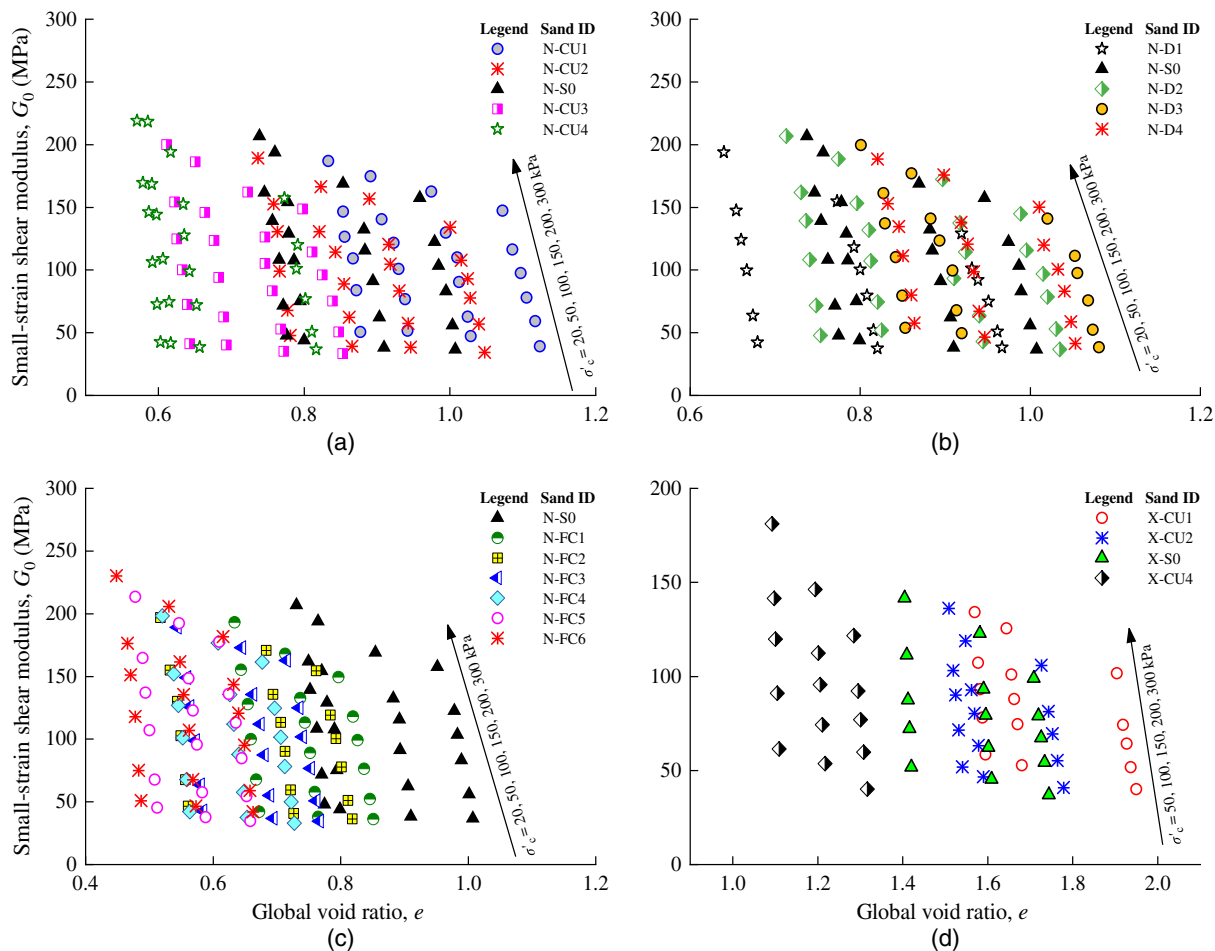


Fig. 6. Variation of G_0 with e for all coral sandy soil specimens in (a) Test group N-CU; (b) Test group N-D; (c) Test group N-FC; and (d) Test group X-CU.

fixed σ'_c (Fig. 6). Table 1 lists the best-fitted values of the material constants A , b , and n in Hardin's equation [for convenience in discussion, which is referred to as Eq. (1) combined with Eq. (3) hereafter] for each coral sandy soil. The n values of the Xisha coral sandy soils were nearly the same as those of the Nansha coral sandy soils, whereas the A and b values of the Xisha coral sandy soils were approximately 2 and 1.5–2 times those of the Nansha coral sandy soils, respectively (Table 1). This indicates that a unique correlation does not exist between G_0 and e for coral sandy soils at different σ'_c .

Fig. 7 plots G_0 versus e of the Nansha coral sandy soils at fixed $\sigma'_c = 100$ kPa, as well as the best-fitting curves by Hardin's equation. The $G_0 - e$ curve moves to the left with increasing C_u [Fig. 7(a)], but moves to the right with increasing d_{50} [Fig. 7(b)]. However, the $G_0 - e$ curve first moves to the left with increasing FC, and then moves to the right as FC exceeds 20% [Fig. 7(c)]. This indicates that, for a given e and σ'_c , G_0 decreases with increasing C_u and decreasing d_{50} , whereas it first decreases and then increases with increasing FC. The power b of the state variable e in Eq. (3) is a constant value, implying that no obvious correlation exists between b and particle gradation parameters (C_u , d_{50} , and FC); this is consistent with the result of Payan et al. (2016).

Fig. 8 shows the correlation between G_0 and e of the Nansha coral sandy soil (Sand ID N-S0) and the Xisha coral sandy soil (Sand ID X-S0) with the same particle-size distribution. The $G_0 - e$ curves of the Xisha coral sandy soil lie to the upper right side of

those of the Nansha coral sandy soil at the same σ'_c , and the maximum value of e for the Nansha coral sandy soil was smaller than the minimum value of e for the Xisha coral sandy soil. This indicates that e cannot be used as a proxy to compare the G_0 values of the Nansha and Xisha coral sandy soils. It also confirms that the correlation between G_0 and e for different coral sandy soils may be different even with identical particle-size distributions, which is attributed to the significantly different particle shapes. This implies that Hardin's equation should not be applied directly for Nansha and Xisha coral sandy soils.

Fig. 9 plots the variation of G_0 versus D_r of the Nansha coral sandy soil (Sand ID N-S0) and the Xisha coral sandy soil (Sand ID X-S0). The $G_0 - D_r$ curves in Fig. 9 were transformed from the corresponding $G_0 - e$ best-fitting curves in Fig. 8 by converting e to D_r . The trends of the $G_0 - D_r$ curves of the Nansha and Xisha coral sandy soils were comparable. For a given σ'_c and D_r , the G_0 values of the Xisha coral sandy soils were 25%–30% less than those of the Nansha coral sandy soils, indicating that the G_0 of the coral sandy soils decreased with the decrease of R . Similar observations were made by Cho et al. (2006) and Payan et al. (2016).

Fig. 10 compares the measured G_0 values of the tested coral sandy soils and the values predicted by the updated Seed's equation. The solid diagonal line in Fig. 10 represents the equality line. Clearly, the difference between predictions and measurements for Nansha coral sandy soils mostly was within 20%. However, for the Xisha coral sandy soils, the G_0 values predicted by the empirical

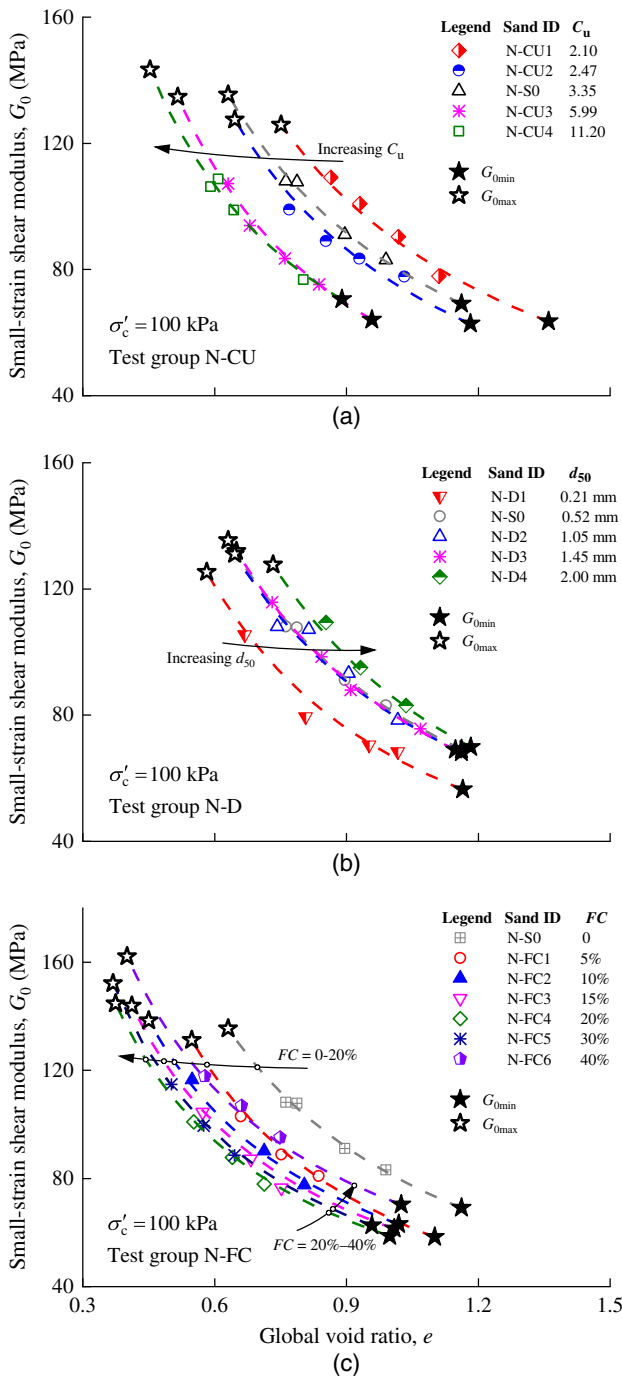


Fig. 7. $G_0 - e$ relationships at $\sigma'_c = 100$ kPa for Nansha coral sandy soils with (a) varying C_u ; (b) varying d_{50} ; and (c) varying FC.

equations were consistently larger than the measured G_0 values by 20%–60%. The possible reason may be that Eqs. (4) and (5) were calibrated using the G_0 values of siliceous sandy soils with round particle shapes. This indicates that the G_0 values of sandy soils may be closely related to the regularity R of soil particles. Consequently, the reliability of the updated Seed's equation is not guaranteed for coral sandy soils with angular and irregular particle shapes.

Unified Formula for G_0

Because the G_0 of each sandy soil decreases with e at constant σ'_c , the minimum small-strain shear modulus G_{0min} corresponding to the

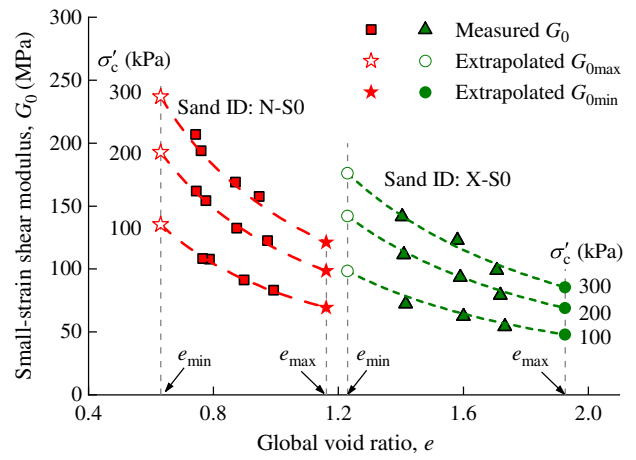


Fig. 8. Variation of G_0 with e for Nansha coral sandy soil (Sand ID N-S0) and Xisha coral sandy soil (Sand ID X-S0).

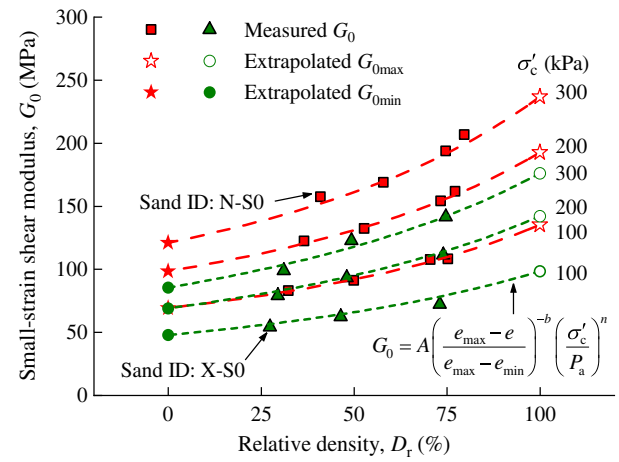


Fig. 9. Variation of G_0 with D_r for Nansha coral sandy soil (Sand ID N-S0) and Xisha coral sandy soil (Sand ID X-S0).

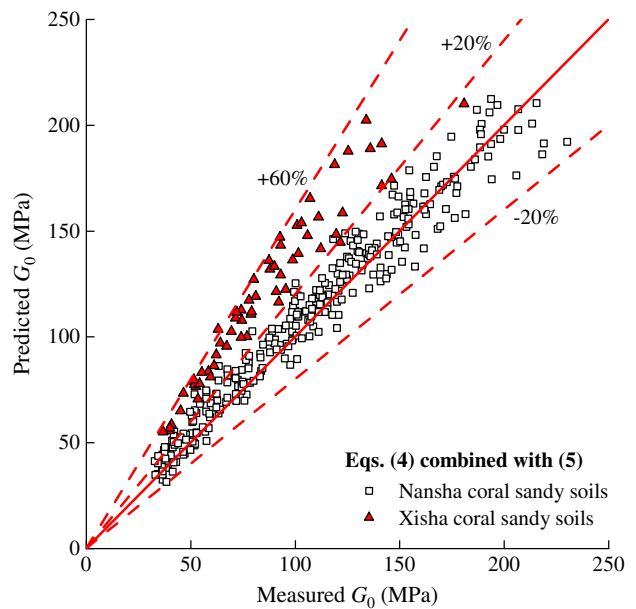


Fig. 10. Measured G_0 and G_0 predicted by the updated Seed's equation for all coral sandy soils tested.

e_{\max} and the maximum small-strain shear modulus $G_{0\max}$ corresponding to the e_{\min} are the lower and upper limits of the G_0 , respectively, which are referred to collectively as the extreme G_0 values. The e value of a specimen continuously decreases during the consolidation processing, so it is impracticable to directly measure the G_0 value of a specimen in the loosest packing state. In addition, because the membrane will be punctured by subangular and angular coral sand particles in the compaction processing, preparation of a specimen in the densest state is very difficult in the laboratory. In this study, the D_r values of the tested specimens ranged between 13% and 90%. The $G_{0\min}$ and $G_{0\max}$ values in Fig. 9 are those determined by extrapolation via Hardin's equation using the best-fitting coefficients (Table 1), as illustrated in Fig. 8.

Fig. 11 plots all the measured G_0 versus e for the 19 coral sandy soils tested at various σ'_c values, together with the data points ($G_{0\max}, e_{\min}$) and ($G_{0\min}, e_{\max}$). At the constant σ'_c , the measured pair of data points (G_0, e) was distributed in a narrow strip. The data points ($G_{0\max}, e_{\min}$) and ($G_{0\min}, e_{\max}$) were located approximately at the upper and lower boundaries of the narrow strip of data points (G_0, e). This implies that the best-fitting curves of data points ($G_{0\max}, e_{\min}$) and ($G_{0\min}, e_{\max}$) can be regarded as the upper and lower boundaries of the measured pair of data points (G_0, e), respectively, which can be expressed as follows:

$$G_{0\max} = 105.02 e_{\min}^{-0.35} \left(\frac{\sigma'_c}{P_a} \right)^{0.49} \quad (9)$$

$$G_{0\min} = 62.59 e_{\max}^{-0.35} \left(\frac{\sigma'_c}{P_a} \right)^{0.49} \quad (10)$$

Therefore, the upper and lower boundaries of the data points (G_0, e) imply the comprehensive influence of the material property indexes C_u , d_{50} , and FC, and the particle shape and mineralogy of sandy soils.

To better analyze the data, a dimensionless constant $G_{0\text{nor}}$ is defined as follows:

$$G_{0\text{nor}} = \frac{G_0 - G_{0\min}}{G_{0\max} - G_{0\min}} \quad (11)$$

Based on Eq. (11), it is expected that $G_{0\text{nor}}$ depends only on e or D_r of the specimen, and the influence of σ'_c is eliminated. Fig. 12(a) shows the variation of $G_{0\text{nor}}$ versus D_r for the Nansha coral sandy soil (Sand ID N-S0) and the Xisha coral sandy soil (Sand ID X-S0). A power-law correlation exists between $G_{0\text{nor}}$ and D_r . Fig. 12(b) plots $G_{0\text{nor}}$ versus D_r for all the tested coral sandy soils. All the data points in Fig. 12(b) are within a very narrow band, implying that a virtually unique correlation exists between $G_{0\text{nor}}$ and D_r regardless of the particle shape, σ'_c , C_u , d_{50} , FC, e_{\min} , and e_{\max} for different sandy soils. The correlation between $G_{0\text{nor}}$ and D_r can be fitted using a power law function, and the fitting result is as follows:

$$G_{0\text{nor}} = D_r^{1.59} \quad (12)$$

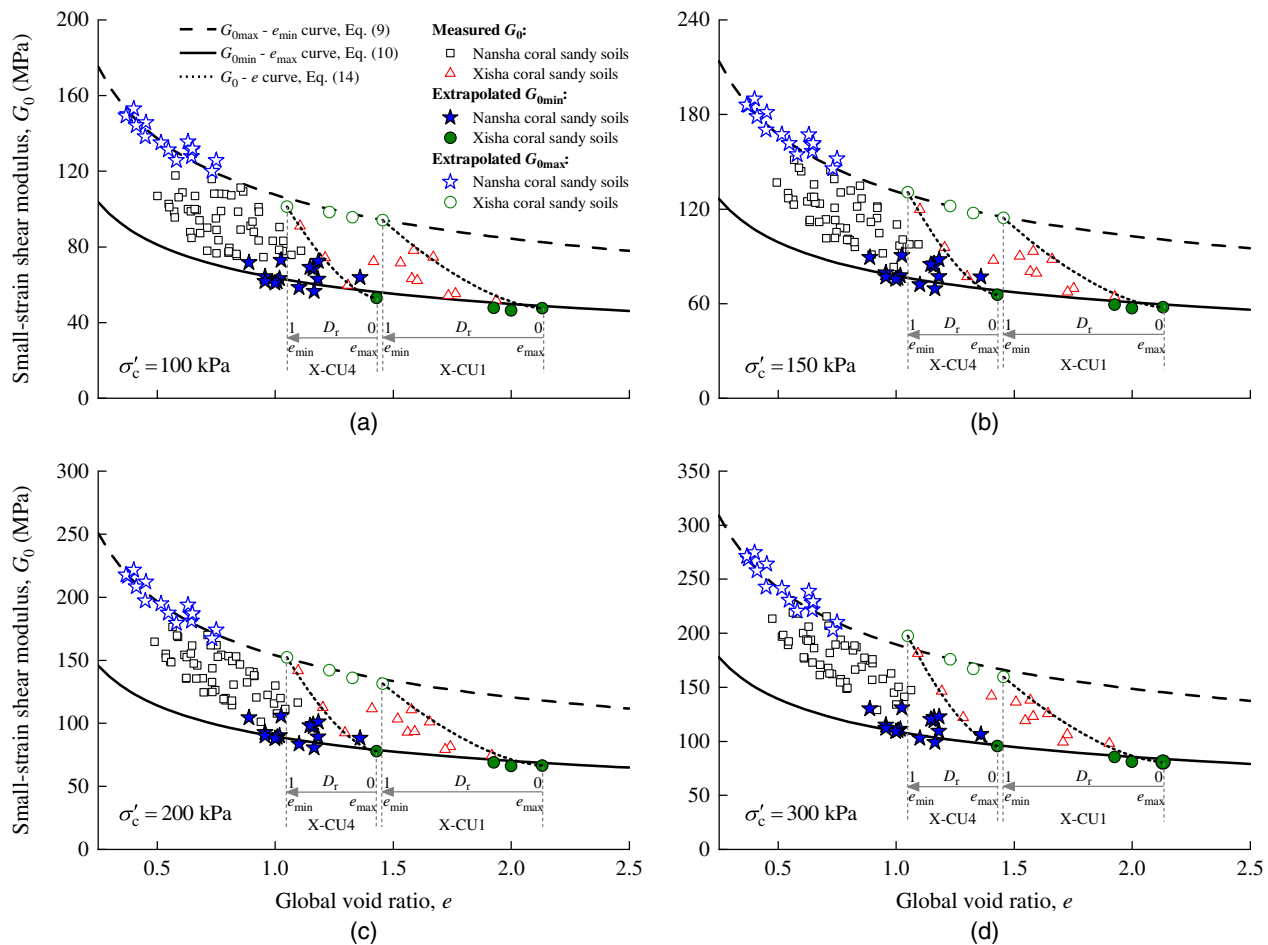


Fig. 11. Variations of G_0 , $G_{0\max}$, and $G_{0\min}$ with e , e_{\min} , and e_{\max} , respectively, for all tested coral sandy soils at (a) $\sigma'_c = 100$ kPa; (b) $\sigma'_c = 150$ kPa; (c) $\sigma'_c = 200$ kPa; and (d) $\sigma'_c = 300$ kPa.

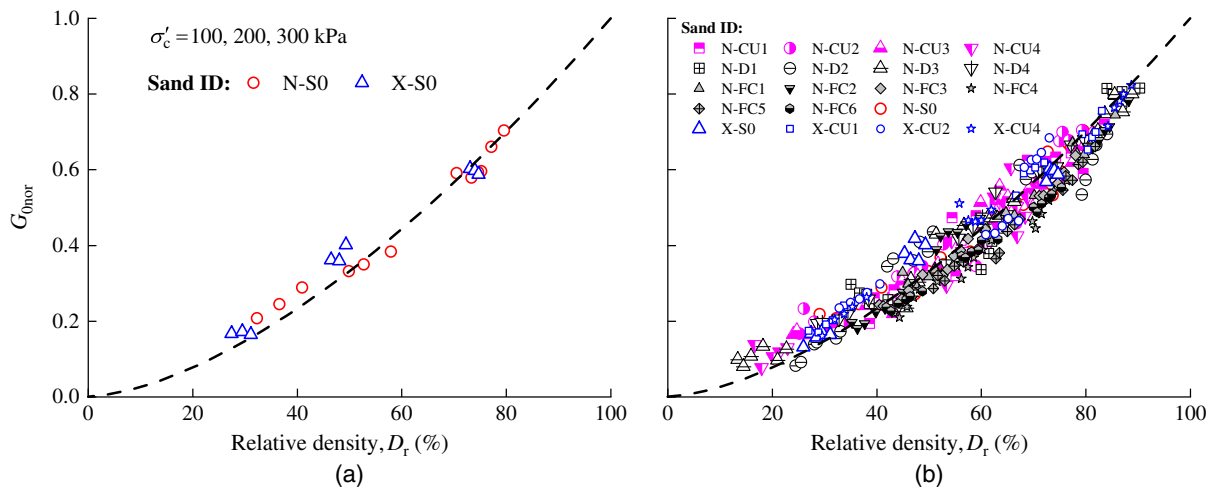


Fig. 12. Variation of G_{0nor} with D_r for (a) Nansha coral sandy soil (Sand ID N-S0) and Xisha coral sandy soil (Sand ID X-S0); and (b) all tested coral sandy soils.

where D_r = decimal form. The R -squared value of fitting is 0.92, indicating a higher reliability of Eq. (12).

The combination of Eqs. (11) and (12) gives

$$G_0 = D_r^{1.59}(G_{0max} - G_{0min}) + G_{0min} \quad (13)$$

Substituting Eqs. (9) and (10) into Eq. (13) gives

$$G_0 = 62.59 \left\{ \left[1.678 \left(\frac{e_{max}}{e_{min}} \right)^{0.35} - 1 \right] D_r^{1.59} + 1 \right\} e_{max}^{-0.35} \left(\frac{\sigma'_c}{P_a} \right)^{0.49} \quad (14)$$

The remarkable merit of Eq. (14) is that the influences of the various factors on G_0 can be accounted for in a simple yet collective manner. For a sandy soil with a specific particle size distribution, e_{min} and e_{max} are fixed, and $D_r = [(e_{max} - e)/(e_{max} - e_{min})]$ is related only to e . Using Eq. (14), the G_0 values at various D_r values can be calculated, ranging between G_{0min} at $D_r = 0$ and G_{0max} at $D_r = 100\%$. The $G_0 - e$ relationship in Eq. (14) by converting D_r to e for two coral sands (X-CU1 and X-CU4) is illustrated in Fig. 11. Thus, G_0 can be predicted easily using Eq. (14). This method is termed the extreme void ratios–based G_0 formula in this study.

Fig. 13 compares the G_0 values predicted by the proposed extreme void ratios–based formula with the measured values for the coral sandy soils. Generally, the deviations between the predicted and the measured G_0 were within 15%, convincingly illustrating the good performance of the proposed formula.

Validation and Discussion

Extensive laboratory element test data of G_0 for sandy soils already exist in the literature. To validate the applicability of the proposed unified G_0 formula [Eq. (14)], a database was established in this study, in which 1,493 relevant test data for various sandy soils with different particle-size distributions, particle shapes, and mineralogies were obtained from 12 references. Of the 1,493 test data validated in this paper, 1,027 were siliceous sandy soil data, 57 were calcareous sandy soil data, and 409 were coral sandy soil data. The basic information of the database and the researchers involved are summarized in Table 2. The specific gravity G_s of 2.65 for the Dorsten siliceous sandy soil in Wichtmann and Triantafyllidis

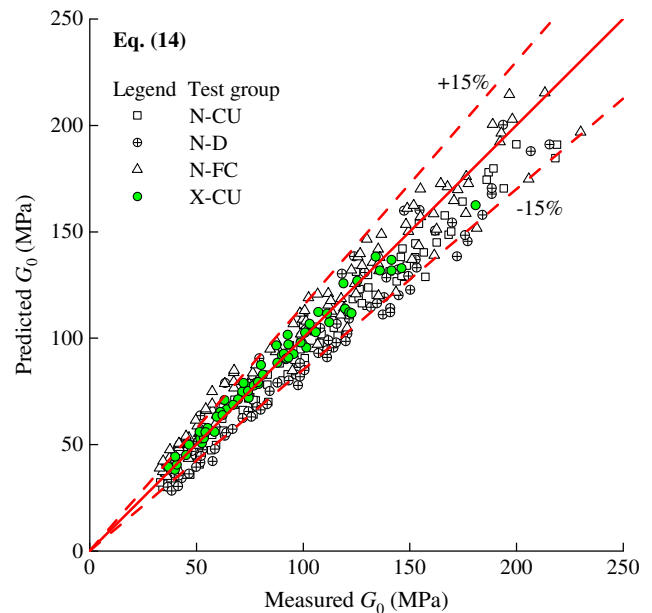


Fig. 13. Measured G_0 and G_0 predicted by Eq. (14) for all tested coral sandy soils.

(2009) was inferred from Lo Presti et al. (1997) and Youn et al. (2008). The values of e_{max} and e_{min} in Senetakis and He (2017) and Liu et al. (2016) also were inferred. In their research, several specimens with various void ratios for each sandy soil were tested. It was assumed that the tested specimens of loosest and densest void ratios (e_L and e_D) for each sandy soil corresponded to specimens of $D_r = 30\%$ and $D_r = 80\%$, respectively. Thus, the e_{max} and e_{min} values can be inferred by solving the following set of equations:

$$(e_{max} - e_L)/(e_{max} - e_{min}) = 30\% \quad (15)$$

$$(e_{max} - e_D)/(e_{max} - e_{min}) = 80\% \quad (16)$$

Fig. 14 summarizes the particle-size distribution curves of the sandy soils in the database. These sandy soils were classified as

Table 2. Summary of basic information of sandy soils in the literature for validating proposed G_0 formula

Reference	Test type	Specimen preparation method	Sandy soil	Particle shape	Sand ID ^a	Index properties						Group symbol (USCS)	
						G_s	C_u	d_{50} (mm)	FC (%)	e_{max}	e_{min}		
Cataño-Arango (2006)	RC	AP	Cabo Rojo calcareous sandy soil	Subangular to angular	—	2.86	2.10	0.38	—	1.560	1.262	SP	
Ha Giang et al. (2017)	BE	MT	Belgian siliceous sandy soil	Round to subangular	Mol	2.64	1.44	0.17	—	0.930	0.581	SP	
						2.79	3.46	0.73	—	1.330	0.903	SP	
						2.79	1.86	0.23	—	1.471	0.933	SP	
						2.79	5.43	0.43	—	0.956	0.508	SP	
						2.79	5.43	0.43	—	1.129	0.652	SP	
						2.79	1.44	0.17	—	1.340	0.843	SP	
Goudarzy et al. (2016)	RC	DT	Hostun quartz sandy soil	—	CHS	2.65	1.96	0.34	—	1.023	0.671	SP	
						2.70	3.43	0.35	—	0.882	0.671	SP	
Jafarian and Javdanian (2020)	RC	AP	Bushehr siliceous-carbonate sandy soil	Angular to subangular	1, 4, 7, 10, 13, 16	2.65	1.39	0.22	—	0.937 ^b	0.631 ^b	SP	
Liu et al. (2016)	RC	DT	Toyoura quartz sandy soil	—	—	2.65	2.92	0.98	—	0.726 ^b	0.484 ^b	SP	
						2.65	2.92	0.98	—	0.726 ^b	0.484 ^b	SP	
Morsy et al. (2019)	RC	AT	Dabaa coral sandy soil	Subrounded to angular	9–12, 19	2.79	2.4	0.31	9.2	1.040	0.750	SP-SM	
Lo Presti et al. (1997)	RC	—	Toyoura quartz sandy soil	—	1–14	2.65	1.35	0.22	—	0.985	0.611	—	
						2.72	4.40	0.75	—	1.281	0.831	—	
						2.68	2.20	0.24	—	0.850	0.592	—	
						2.67	1.58	0.27	—	1.008	0.608	SP	
Senetakakis et al. (2012)	RC	DT	Quartz siliceous sandy soil	Subrounded	N1	2.67	2.76	0.56	—	0.841	0.467	SP	
						2.67	1.34	0.60	—	0.963	0.628	SP	
						2.67	1.70	0.23	—	1.630 ^b	1.118 ^b	SP	
Senetakakis and He (2017)	RC	—	Western Australia carbonate sandy soil	Subangular	BS-1–BS-3	2.81	3.83	0.60	0	1.188	0.728	SP	
Shi et al. (2020)	BE	DT	Persian Gulf coral sand–fines mixtures	Subangular to angular	S1	2.81	3.83	0.60	0	1.188	0.728	SP	
						S1 + 10%FC	2.81	—	—	10	1.127	0.604	SW-SM
						S1 + 20%FC	2.80	—	—	20	0.988	0.516	SP-SM
						S1 + 30%FC	2.80	—	—	30	0.946	0.498	SW-SM
						S1 + 40%FC	2.79	—	—	40	1.051	0.517	SW-SM
						S1 + 50%FC	2.79	—	—	50	1.067	0.576	SW-SM
Wichtmann and Triantafyllidis (2009)	RC	AP	Dorsten quartz sandy soil	Subangular	L2	2.76	—	—	100	1.649	0.993	SM	
						2.65 ^b	1.5	0.2	—	0.994	0.595	SP	
						2.65 ^b	1.5	0.6	—	0.892	0.571	SP	
						2.65 ^b	1.5	2.0	—	0.877	0.591	SP	
						2.65 ^b	2.0	0.6	—	0.865	0.542	SP	
						2.65 ^b	2.5	0.6	—	0.856	0.495	SP	
						2.65 ^b	3.0	0.6	—	0.829	0.474	SP	
						2.65 ^b	5.0	0.6	—	0.748	0.395	SP	
						2.65 ^b	8.0	0.6	—	0.673	0.356	SP	
						2.65 ^b	2.0	2.0	—	0.826	0.554	SP	
						2.65 ^b	2.5	2.0	—	0.810	0.513	SP	
						2.65 ^b	3.0	2.0	—	0.783	0.491	SP	
						2.65 ^b	5.0	2.0	—	0.703	0.401	SP	
						2.65 ^b	8.0	2.0	—	0.520	0.398	SP	
Youn et al. (2008)	RC, BE, TS	AP	Toyoura quartz sandy soil	—	—	2.65	1.29	0.20	—	0.982	0.617	SP	
						2.63	2.01	0.16	—	0.854	0.642	SP	
						2.63	2.01	0.16	—	0.854	0.642	SP	
						2.63	2.01	0.16	—	0.854	0.642	SP	
						2.63	2.01	0.16	—	0.854	0.642	SP	
						2.63	2.01	0.16	—	0.854	0.642	SP	

Note: RC = resonant column test; BE = bender element test; TS = torsional shear test; AP = air pluviation; DT = dry tamping; MT = moist tamping; and USCS = Unified Soil Classification System.

^aSand ID copied from the original paper.

^bConjectural value.

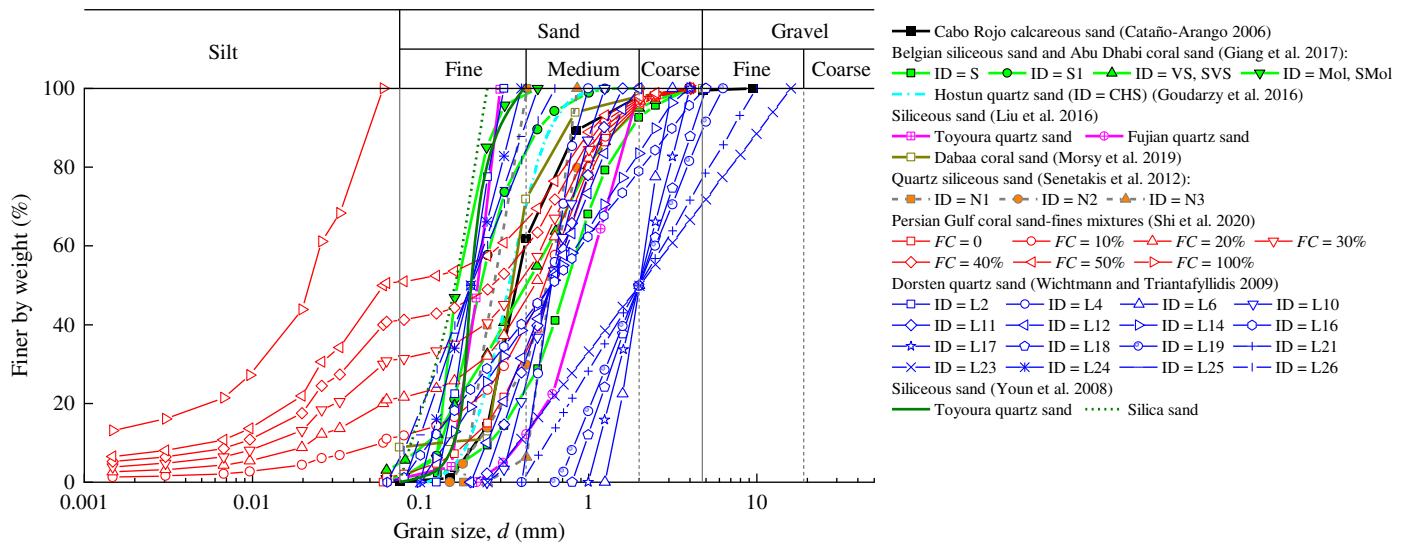


Fig. 14. Particle-size distribution curves of sandy soils collected from the literature.

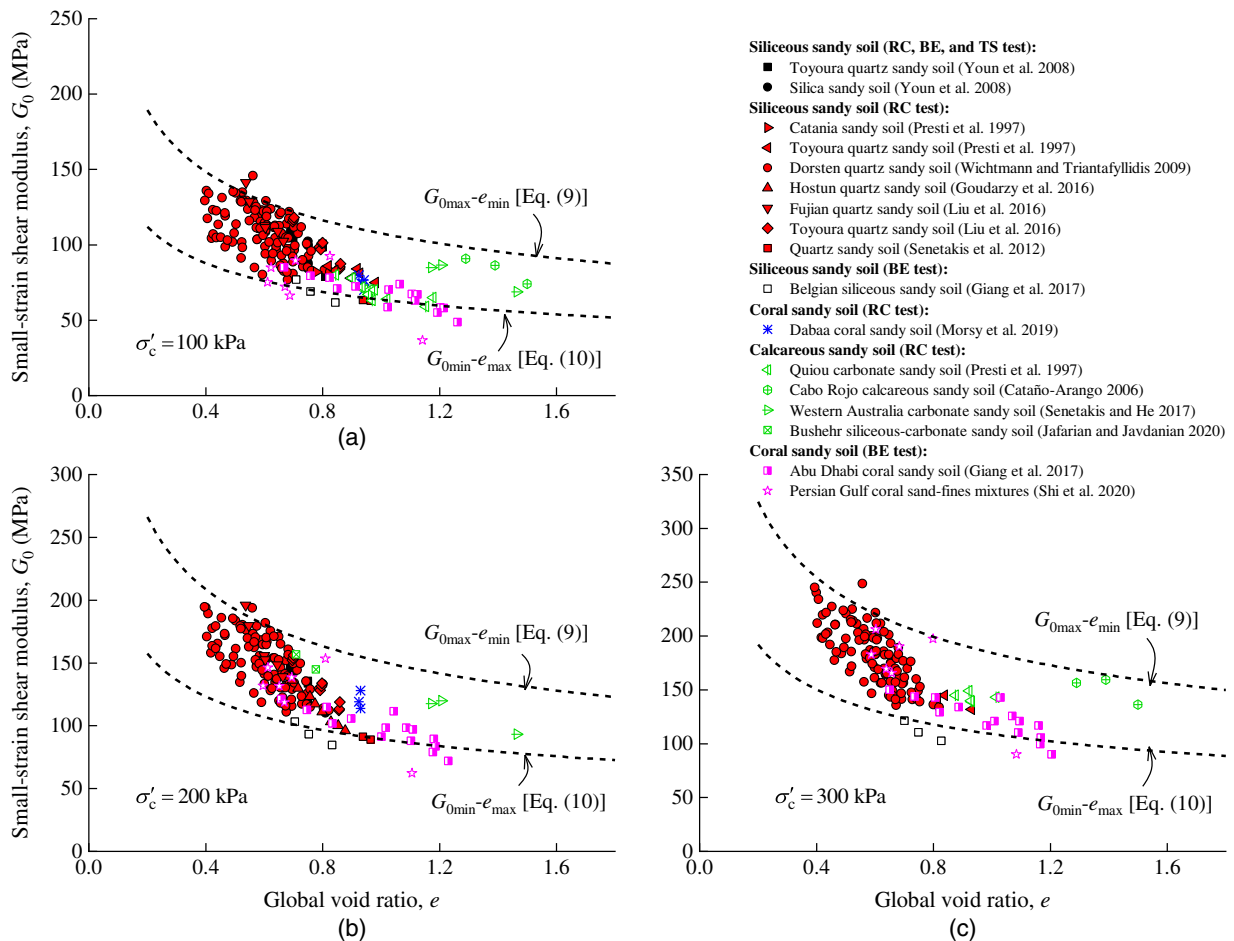


Fig. 15. Variations of G_0 with e for all sandy soils in the literature at (a) $\sigma'_c = 100$ kPa; (b) $\sigma'_c = 200$ kPa; and (c) $\sigma'_c = 300$ kPa.

poorly graded sand and poorly graded sand with gravel (SP), poorly graded sand with silt (SP-SM), well-graded sand with silt (SW-SM), and silty sand (SM), according to the Unified Soil Classification System (ASTM 2011) (Table 2).

Fig. 15 plots the G_0 data versus e compiled from the database. All the G_0 data were located in a range between the upper and lower boundaries determined by Eqs. (9) and (10), respectively (Fig. 15). Approximately 64.5%, 33.5%, and 2% of the database were from

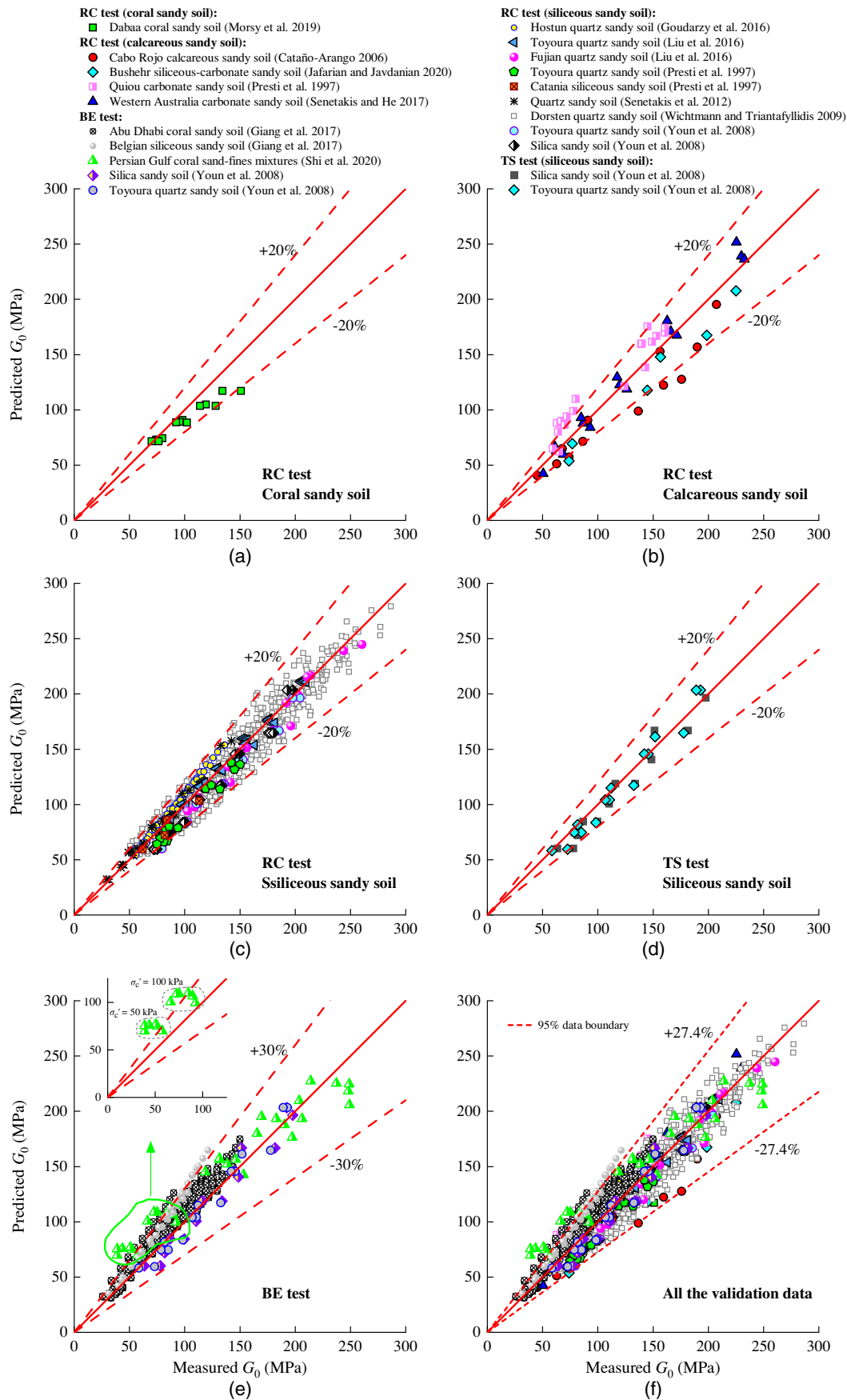


Fig. 16. Measured G_0 values using data from the literature and values predicted by the proposed extreme void ratios–based G_0 formula: (a) coral sandy soils tested by RC test; (b) calcareous sandy soils tested by RC test; (c) siliceous sandy soils tested by RC test; (d) siliceous (quartz) sandy soils tested by TS test; (e) sandy soils tested by BE test; and (f) all validation data.

RC, BE, and torsional shear (TS) tests. Although the G_0 database was collected from various testing methods, there was no dramatic difference between the upper and lower boundaries among the compiled G_0 data obtained from various tests.

Fig. 16 compares the measured G_0 values of various sandy soils compiled from the database and the values predicted by the proposed extreme void ratios-based G_0 formula [Eq. (14)]. The deviation between the predicted and the measured G_0 values were within a range of $\pm 20\%$ for data from RC and TS tests [Figs. 16(a–d)]. This prediction was slightly weaker than the prediction of the tested coral sandy soils (Fig. 13), but still satisfactory. Bayat and Ghalandarzadeh (2019) investigated the influence of the specimen preparation methods on the G_0 of sand, and found that the G_0 of the specimens prepared by the moist tapping (MT) method was the largest, followed by the dry deposition (DD) method, and the smallest G_0 was for the water sedimentation (WS) method. Gu et al. (2015) showed that the G_0 values of the specimens prepared by the MT method from RC and TS tests are about 6%–7% higher than those of the air pluviation (AP) and dry tamping (DT) specimens. Because the G_0 values in the literature data were measured by different apparatuses and operators at different specimen preparation conditions, inherent discrepancies exist among the measured G_0 values in the literature data. Hence, the reliability of the proposed G_0 formula in this paper is convincingly confirmed. Fig. 16(e) compares the measured and predicted G_0 data from the BE tests. The predicted G_0 values of the siliceous sandy soils in Youn et al. (2008) agree very well with the measured values. However, the proposed G_0 formula overestimated the G_0 values of the coral sandy soils in Ha Giang et al. (2017) and Shi et al. (2020), especially the G_0 values in the cases of $\sigma'_c = 50$ and 100 kPa in Shi et al. (2020), and the deviation between the predicted and the measured G_0 values generally was within $\pm 30\%$, which is higher than the deviations for the RC and TS tests.

Many researchers have concluded that the largest uncertainty and difficulty of BE tests lie in the determination of the travel time of the shear wave (Jovicic et al. 1996; Lee and Santamarina 2005; Yamashita et al. 2009; Yang and Gu 2013; Gu et al. 2015).

Yang and Gu (2013) showed that the measured G_0 increases with the ratio of wavelength (λ) to d_{50} for the peak-to-peak method, whereas it decreases with the increase of λ/d_{50} for the start-to-start method. Shi et al. (2020) adopted the peak-to-peak method to determine the arrival time in multidirectional BE tests with an excitation frequency of 15 kHz, and there is a potential effect of anisotropy on the value of G_0 . The results indicated that the measured G_0 values of the coral sandy soil are smaller than those of siliceous sandy soils at $\sigma'_c < 100$ kPa, for which the calibrated stress power n in Eq. (1) ranging from 0.63 to 0.77 for the coral sandy soil was larger than the typical range of 0.35–0.7 for siliceous sandy soils. In addition, the G_0 values determined by the peak-to-peak method were confirmed to be smaller than those from RC tests (Yang and Gu 2013). Ha Giang et al. (2017) used the start-to-start method to determine the shear wave travel time through specimens prepared by moist tamping in BE tests with an excitation frequency of 10 kHz. The uncertainty of this method is relatively high because it is difficult to determine the inflection point representing the first arrival in the received wave due to the near-field and side-reflected compressional waves. Yamashita et al. (2009) deduced from international round robin test results that the scatter of measured G_0 values in BE tests was higher in DT specimens than in saturated specimens. The G_0 values measured by BE tests for MT specimens were about 20% higher than those of the specimens prepared using the AP and DT methods, and the difference was much larger for BE tests than for RC and TS tests (De Alba et al. 1984; Gu et al. 2015). Compared with the DT and AP methods, the MT method requires much more compaction energy to achieve the same e due to the induced capillary force occurring in the moist state. This implies that different specimen preparation methods result in different soil structures at the same e and σ'_c . Furthermore, the BE test measures the local stiffness of a specimen along the wave travel path, whereas the RC and TS tests measure the global (average) stiffness of whole specimen. In addition, Fig. 16(f) compares the predicted and measured G_0 values for all the data from the literature. The prediction bounds for capturing 94.2% of the data are $\pm 25\%$ deviation lines.

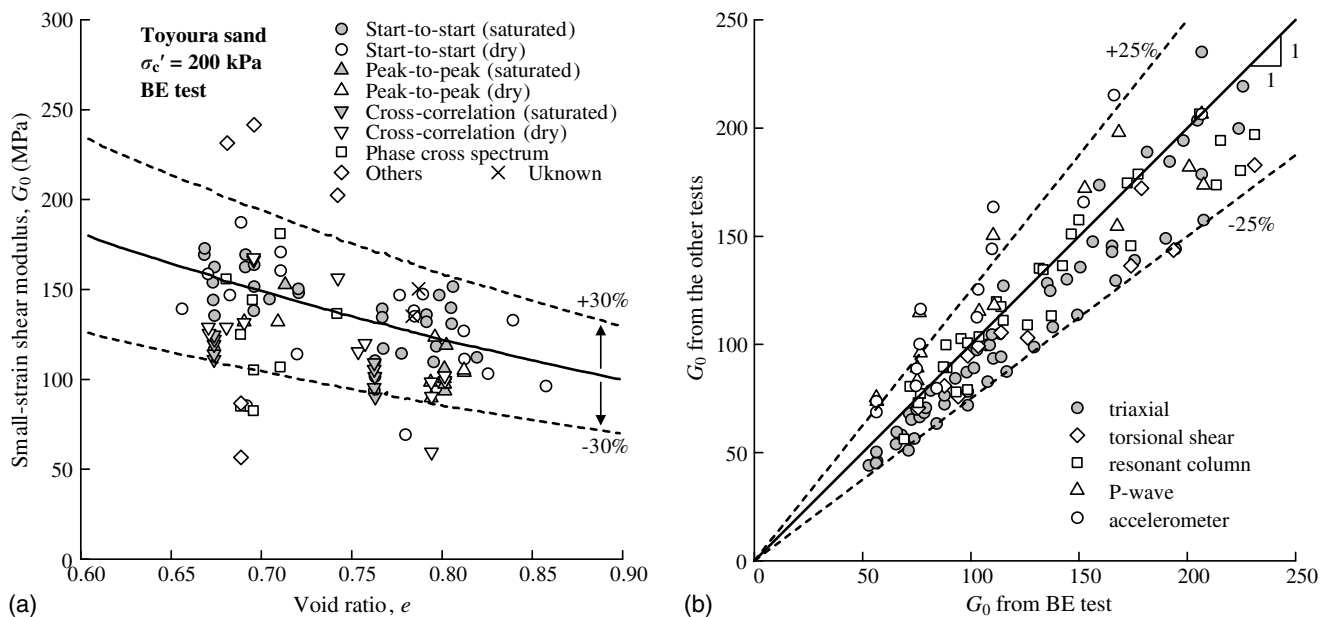


Fig. 17. International parallel test results of G_0 (redrawn from Yamashita et al. 2009) for (a) $G_0 - e$ relationship from the BE test by various determination methods of shear wave travel time; and (b) G_0 values from the BE test and other types of test. [Reprinted from Yamashita et al. (2009), under Creative Commons-BY-4.0 license (<https://creativecommons.org/licenses/by-nc-nd/4.0/>).]

Fig. 17 shows the G_0 values measured by various BE tests, and compares the G_0 values from BE tests with those from other types of tests of Toyoura sand (Yamashita et al. 2009). There was a great deal of scatter of measured G_0 values, up to 30% or more, in different BE tests [Fig. 17(a)]. The G_0 values from measured BE tests and from other types of tests matched well, with a significant deviation of up to 25% or more [Fig. 17(b)]. Given the inherent discrepancies among the G_0 values using different signal interpretation methods and the effect of sample preparation method in BE tests, the performance of the proposed G_0 formula for the data from BE tests also is acceptable.

Fig. 18 presents the statistics of relative errors between the predicted and measured G_0 values of various sandy soils in the database. The absolute relative error (ARR) is defined as

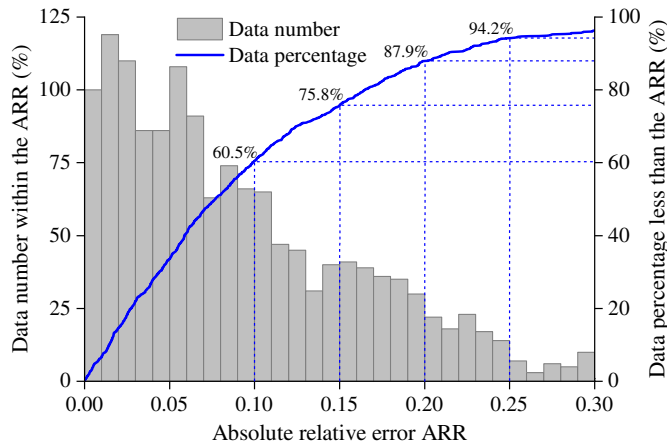


Fig. 18. Statistics of the absolute relative errors between measured and predicted G_0 values using the literature database.

$$ARR(\%) = \left| \frac{\text{measured } G_0 - \text{predicted } G_0}{\text{measured } G_0} \right| \times 100\% \quad (17)$$

The proportions of data points with ARR less than 10%, 15%, 20%, and 25% were 60.5%, 75.8%, 87.9%, and 94.2%, respectively. The mean ARR value for all the data was 10.4%. Because of the effects of different specimen preparation methods, testing apparatuses and principles, test details, signal interpretations, and so on, the G_0 values obtained from different methods cannot be expected to be almost the same. Although the particle gradation and shape and mineralogy of the tested sandy soils in this study and in the literature were different and the physical state indexes and material properties varied greatly, Figs. 16 and 18 indicate that the proposed G_0 formula can be used to predict the G_0 value of a wide range of sandy soils in a simple, generic, and yet reliable way. This suggests that the proposed equation works reasonably and robustly well for a wide range of sandy soils with various particle shapes, mineralogies, and particle-size distributions.

The upper-limit value of e_{\max} and the lower-limit value of e_{\min} of various siliceous sandy soils in previous studies were about 1.0 and 0.4, respectively, whereas the values of $(e_{\max} - e_{\min})$ were in the range 0.25–0.65 (e.g., Iwasaki and Tatsuoka 1977; Seed et al. 1986; Menq 2003; Wichtmann and Triantafyllidis 2009; Payan et al. 2016). Therefore, significant differences in e_{\max} , e_{\min} , and $(e_{\max} - e_{\min})$ exist between siliceous sandy soils and coral sandy soils. Whether the G_0 formulas developed mainly for siliceous sandy soils in the literature are applicable for coral sandy soils is a concern. Fig. 19 compares the G_0 values predicted using the formula proposed by Payan et al. (2016) and using the formula proposed by Menq (2003) with the measured G_0 values for the coral sandy soils in this study. The formula of Payan et al. (2016) considers the effects of σ'_c , C_u , e , and particle shape, whereas the formula of Menq (2003) considered the effects of σ'_c , C_u , d_{50} , and e . Both formulas significantly underestimated the G_0 values of coral

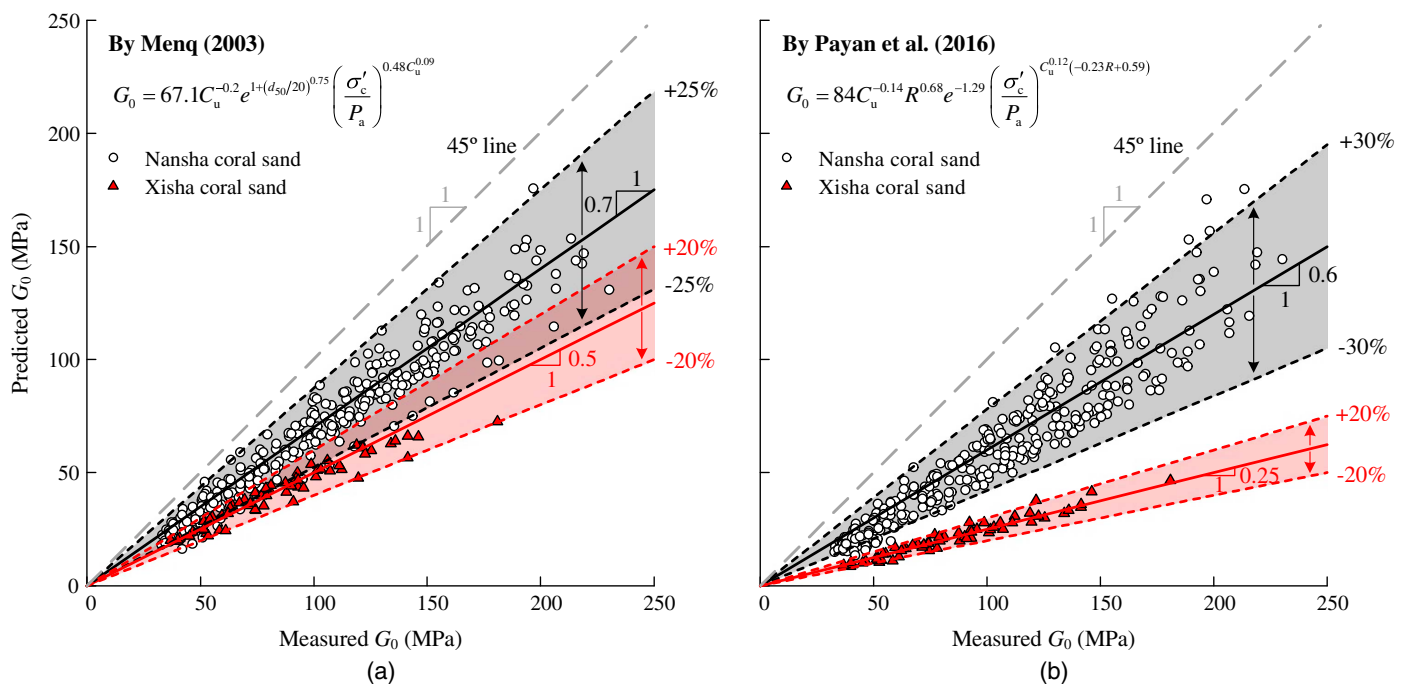


Fig. 19. Measured and predicted G_0 values for the tested Nansha and Xisha coral sands using equations of (a) Menq (2003); and (b) Payan et al. (2016).

sands, particularly Xisha coral sand (Fig. 19). Therefore caution should be taken when using the formulas for coral sands.

Conclusion

A series of RC tests was conducted on Nansha and Xisha coral sands of various gradings, focusing on the material and physical properties that may affect the small-strain shear modulus G_0 . The main conclusions and findings are summarized as follows:

1. The G_0 value of a coral sand is affected significantly by its particle-size distribution and particle shape. For constant e and σ'_c , G_0 decreases as C_u increases, and increases as d_{50} increases, respectively. However, G_0 first decreases and then increases with FC, and reaches a minimum value at a FC of approximately 20%. For constant σ'_c and D_r , the G_0 of the Xisha coral sands was 25%–30% smaller than that of the Nansha coral sands.
2. The extreme void ratios (e_{\max} and e_{\min}) of sandy soils are intrinsic properties that collectively reflect the effects of various factors such as particle-size distribution and particle shape of coral sands. At a constant σ'_c , the maximum and minimum small-strain shear modulus ($G_{0\max}$ and $G_{0\min}$) decrease in a power function form [Eqs. (9) and (10)] as e_{\min} and e_{\max} increase. An explicit empirical formula [Eq. (14)] is proposed to predict G_0 that is a simple function of e_{\max} , e_{\min} , D_r , and σ'_c . Eq. (14) captures the effects of various factors on G_0 in a simple yet collective manner.
3. A large database of G_0 of siliceous, carbonate, and coral sands was compiled from the literature. The deviations between the G_0 predicted using the proposed formula [Eq. (14)] and the measured G_0 were within 20% for data from RC and TS tests and 30% for data from BE tests. The mean value of absolute relative errors for all the G_0 data in this database was 10.4%, indicating a wide applicability of the proposed formula.
4. Because of the large differences of extreme void ratios (both e_{\max} and e_{\min}) between siliceous sandy soils and coral sandy soils, further examination of the applicability of the proposed G_0 formulas using experimental data for other sandy soils would be worthwhile.

Data Availability Statement

All data, models, and code generated or used during the study appear in the published article.

Acknowledgments

The financial support provided by the National Natural Science Foundation of China (51978334 and 52278503), the Research Grants Council of Hong Kong (17206119), and the Beijing Natural Science Foundation (8224082) is gratefully acknowledged.

References

- Åberg, B. 1992. "Void ratio of noncohesive soils and similar materials." *J. Geotech. Eng.* 118 (9): 1315–1334. [https://doi.org/10.1061/\(ASCE\)0733-9410\(1992\)118:9\(1315\)](https://doi.org/10.1061/(ASCE)0733-9410(1992)118:9(1315)).
- Åberg, B. 1996. "Grain-size distribution for smallest possible void ratio." *J. Geotech. Eng.* 122 (1): 74–77. [https://doi.org/10.1061/\(ASCE\)0733-9410\(1996\)122:1\(74\)](https://doi.org/10.1061/(ASCE)0733-9410(1996)122:1(74)).
- Altuhafi, F. N., M. R. Coop, and V. N. Georgiannou. 2016. "Effect of particle shape on the mechanical behavior of natural sands." *J. Geotech.*

- Environ. Eng.* 142 (12): 04016071. [https://doi.org/10.1061/\(ASCE\)GT.1943-5606.0001569](https://doi.org/10.1061/(ASCE)GT.1943-5606.0001569).
- ASTM. 2011. *Standard practice for classification of soils for engineering purposes (unified soil classification system)*. ASTM D2487. West Conshohocken, PA: ASTM.
- ASTM. 2013. *Standard test methods for the determination of the modulus and damping properties of soils using the cyclic triaxial apparatus*. ASTM D3999/D3999M. West Conshohocken, PA: ASTM.
- ASTM. 2016a. *Standard test methods for maximum index density and unit weight of soils using a vibratory table*. ASTM D4253. West Conshohocken, PA: ASTM.
- ASTM. 2016b. *Standard test methods for minimum index density and unit weight of soils and calculation of relative density*. ASTM D4254. West Conshohocken, PA: ASTM.
- Atkinson, J. H., and G. Salfors. 1991. "Experimental determination of soil properties." In *Proc., 10th European Conf. on Soil Mechanics and Foundation Engineering*, 915–956. New York: A.A. Balkema.
- Bayat, M., and A. Ghalandarzadeh. 2019. "Influence of depositional method on dynamic properties of granular soil." *Int. J. Civ. Eng.* 17 (6): 907–920. <https://doi.org/10.1007/s40999-019-00412-7>.
- Bellotti, R., M. Jamiolkowski, D. C. F. Lo Presti, and D. A. O'Neill. 1996. "Anisotropy of small strain stiffness in Ticino sand." *Géotechnique* 46 (1): 115–131. <https://doi.org/10.1680/geot.1996.46.1.115>.
- Brandes, H. G. 2011. "Simple shear behavior of calcareous and quartz sands." *Geotech. Geol. Eng.* 29 (1): 113–126. <https://doi.org/10.1007/s10706-010-9357-x>.
- Bui, M. T. 2009. "Influence of some particle characteristics on the small strain response of granular materials." Doctoral dissertation, School of Civil Engineering and the Environment, Univ. of Southampton.
- Cataño-Arango, J. 2006. "Stress strain behavior and dynamic properties of Cabo Rojo calcareous sands." M.Sc thesis, Dept. of Civil Engineering, Univ. of Puerto Rico.
- Chang, C. S., Y. Deng, and Z. Yang. 2017. "Modeling of minimum void ratio for granular soil with effect of particle size distribution." *J. Eng. Mech.* 143 (9): 04017060. [https://doi.org/10.1061/\(ASCE\)EM.1943-7889.0001270](https://doi.org/10.1061/(ASCE)EM.1943-7889.0001270).
- Chang, C. S., J. Y. Wang, and L. Ge. 2016. "Maximum and minimum void ratios for sand-silt mixtures." *Eng. Geol.* 211 (23): 7–18. <https://doi.org/10.1016/j.enggeo.2016.06.022>.
- Chen, G., Q. Wu, T. Sun, K. Zhao, E. Zhou, L. Xu, and Y. Zhou. 2021a. "Cyclic behaviors of saturated sand-gravel mixtures under undrained cyclic triaxial loading." *J. Earthquake Eng.* 25 (4): 756–789. <https://doi.org/10.1080/13632469.2018.1540370>.
- Chen, G. X., K. Liang, K. Zhao, and J. Yang. 2022. "Shear modulus and damping ratio of saturated coral sand under generalised cyclic loadings." *Géotechnique* 1 (Jan): 18. <https://doi.org/10.1680/jgeot.21.00181>.
- Chen, G. X., W. J. Ma, Y. Qin, K. Zhao, and J. Yang. 2021b. "Liquefaction susceptibility of saturated coral sand subjected to various patterns of principal stress rotation." *J. Geotech. Geoenviron. Eng.* 147 (9): 04021093. [https://doi.org/10.1061/\(ASCE\)GT.1943-5606.0002590](https://doi.org/10.1061/(ASCE)GT.1943-5606.0002590).
- Chen, G. X., Y. Z. Wang, D. F. Zhao, K. Zhao, and J. Yang. 2021c. "A new effective stress method for nonlinear site response analyses." *Earthquake Eng. Struct. Dyn.* 50 (6): 1595–1611. <https://doi.org/10.1002/eqe.3414>.
- Chen, G. X., Q. Wu, K. Zhao, Z. F. Shen, and J. Yang. 2020. "A binary packing material-based procedure for evaluating soil liquefaction triggering during earthquakes." *J. Geotech. Geoenviron. Eng.* 146 (6): 04020040. [https://doi.org/10.1061/\(ASCE\)GT.1943-5606.0002263](https://doi.org/10.1061/(ASCE)GT.1943-5606.0002263).
- Chen, G. X., D. F. Zhao, W. Y. Chen, and C. H. Juang. 2019a. "Excess pore-water pressure generation in cyclic undrained testing." *J. Geotech. Geoenviron. Eng.* 145 (7): 04019022. [https://doi.org/10.1061/\(ASCE\)GT.1943-5606.0002057](https://doi.org/10.1061/(ASCE)GT.1943-5606.0002057).
- Chen, G. X., Z. L. Zhou, H. Pan, T. Sun, and X. J. Li. 2016. "The influence of undrained cyclic loading patterns and consolidation states on the deformation features of saturated fine sand over a wide strain range." *Eng. Geol.* 204 (14): 14–22. <https://doi.org/10.1016/j.enggeo.2016.02.008>.
- Chen, G. X., Z. L. Zhou, T. Sun, Q. Wu, L. Y. Xu, S. Khoshnevisan, and D. S. Ling. 2019b. "Shear modulus and damping ratio of sand-gravel

- mixtures over a wide strain range." *J. Earthquake Eng.* 23 (8): 1407–1440. <https://doi.org/10.1080/13632469.2017.1387200>.
- Cheng, L., M. S. Hossain, Y. Hu, Y. H. Kim, and S. N. Ullah. 2022. "A simple breakage model for calcareous sand and its FE implementation." *J. Geotech. Geoenviron. Eng.* 148 (9): 04022065. [https://doi.org/10.1061/\(ASCE\)GT.1943-5606.0002834](https://doi.org/10.1061/(ASCE)GT.1943-5606.0002834).
- Cho, G.-C., J. Dodds, and J. C. Santamarina. 2006. "Particle shape effects on packing density, stiffness, and strength: Natural and crushed sands." *J. Geotech. Geoenviron. Eng.* 133 (5): 591–602. [https://doi.org/10.1061/\(ASCE\)1090-0241\(2006\)132:5\(591\)](https://doi.org/10.1061/(ASCE)1090-0241(2006)132:5(591)).
- Clayton, C. R. I. 2011. "Stiffness at small strain: Research and practice." *Géotechnique* 61 (1): 5–37. <https://doi.org/10.1680/geot.2011.61.1.5>.
- Clayton, C. R. I., and G. Heymann. 2001. "Stiffness of geomaterials at very small strains." *Géotechnique* 51 (3): 245–255. <https://doi.org/10.1680/geot.2001.51.3.245>.
- Coop, M. R., K. K. Sorensen, T. Bodas Freitas, and G. Georgoutsos. 2004. "Particle breakage during shearing of a carbonate sand." *Géotechnique* 54 (3): 157–163. <https://doi.org/10.1680/geot.2004.54.3.157>.
- Cubrinovski, M., and K. Ishihara. 1999. "Empirical correlation between SPT N -value and relative density for sandy soils." *Soils Found.* 39 (5): 61–71. https://doi.org/10.3208/sandf.39.5_61.
- Cubrinovski, M., and K. Ishihara. 2002. "Maximum and minimum void ratio characteristics of sands." *Soils Found.* 42 (6): 65–78. https://doi.org/10.3208/sandf.42.6_65.
- Darvasi, Y. 2021. "Shear-wave velocity measurements and their uncertainties at six industrial sites." *Earthquake Spectra* 37 (3): 2223–2246. <https://doi.org/10.1177/8755293020988029>.
- De Alba, P., K. Baldwin, V. Janoo, G. Roe, and B. Celikkol. 1984. "Elastic-wave velocities and liquefaction potential." *Geotech. Test. J.* 7 (2): 77–87. <https://doi.org/10.1520/GTJ10596J>.
- Einav, I. 2007. "Breakage mechanics—Part I: Theory." *J. Mech. Phys. Solids* 55 (6): 1274–1297. <https://doi.org/10.1016/j.jmps.2006.11.003>.
- Flores Lopez, F. A., V. M. Taboada, Z. X. Gonzalez Ramirez, D. Cruz Roque, P. Barrera Nabor, and V. S. Dantal. 2018. "Normalized modulus reduction and damping ratio curves for Bay of Campeche carbonate sand." In *Proc., Offshore Technology Conf.* Houston: Offshore Technology Conference.
- GCTS (Geotechnical Consulting and Testing Systems). 2014. *TSH-100 resonant column/torsional shear technical information manual*. Tempe, AZ: GCTS.
- Goudarzy, M., M. M. Rahman, D. König, and T. Schanz. 2016. "Influence of non-plastic fines content on maximum shear modulus of granular materials." *Soils Found.* 56 (6): 973–983. <https://doi.org/10.1016/j.sandf.2016.11.003>.
- Gu, X. Q., L. T. Lu, and J. G. Qian. 2017. "Discrete element modeling of the effect of particle size distribution on the small strain stiffness of granular soils." *Particuology* 32 (Aug): 21–29. <https://doi.org/10.1016/j.partic.2016.08.002>.
- Gu, X. Q., and J. Yang. 2013. "A discrete element analysis of elastic properties of granular materials." *Granular Matter* 15 (2): 139–147. <https://doi.org/10.1007/s10035-013-0390-3>.
- Gu, X. Q., J. Yang, M. Huang, and G. Gao. 2015. "Bender element tests in dry and saturated sand: Signal interpretation and result comparison." *Soils Found.* 55 (5): 951–962. <https://doi.org/10.1016/j.sandf.2015.09.002>.
- Gu, X. Q., J. Yang, and M. S. Huang. 2013. "Laboratory measurements of small strain properties of dry sands by bender element." *Soils Found.* 53 (5): 735–745. <https://doi.org/10.1016/j.sandf.2013.08.011>.
- Ha Giang, P. H., P. O. Van Impe, W. F. Van Impe, P. Mengesha, and W. Haegeman. 2017. "Small-strain shear modulus of calcareous sand and its dependence on particle characteristics and gradation." *Soil Dyn. Earthquake Eng.* 100 (Jun): 371–379. <https://doi.org/10.1016/j.soildyn.2017.06.016>.
- Hardin, B. O. 1985. "Crushing of soil particles." *J. Geotech. Eng.* 111 (10): 1177–1192. [https://doi.org/10.1061/\(ASCE\)0733-9410\(1985\)111:10\(1177\)](https://doi.org/10.1061/(ASCE)0733-9410(1985)111:10(1177)).
- Hardin, B. O., and W. L. Black. 1966. "Sand stiffness under various triaxial stresses." *J. Soil Mech. Found. Div.* 92 (2): 27–42. <https://doi.org/10.1061/JSFEAQ.0000865>.
- Hardin, B. O., and F. E. Richart Jr. 1963. "Elastic wave velocities in granular soils." *J. Soil Mech. Found. Div.* 89 (1): 33–65. <https://doi.org/10.1061/JSFEAQ.0000493>.
- Ishihara, K. 1996. *Soil behaviour in earthquake geotechnics*. Oxford, UK: Clarendon.
- Iwasaki, T., and F. Tatsuoka. 1977. "Effects of grain size and grading on dynamic shear moduli of sands." *Soils Found.* 17 (3): 19–35. https://doi.org/10.3208/sandf1972.17.3_19.
- Jafarian, Y., and H. Javdanian. 2020. "Dynamic properties of calcareous sand from the Persian Gulf in comparison with siliceous sands database." *Int. J. Civ. Eng.* 18 (2): 245–249. <https://doi.org/10.1007/s40999-019-00402-9>.
- Jovicic, V., M. R. Coop, and M. Simic. 1996. "Objective criteria for determining G_{max} from bender element tests." *Géotechnique* 46 (2): 357–362. <https://doi.org/10.1680/geot.1996.46.2.357>.
- Kokusho, T. 1980. "Cyclic triaxial test of dynamic soil properties for wide strain range." *Soils Found.* 20 (2): 45–60. https://doi.org/10.3208/sandf1972.20.2_45.
- Krumbein, W. C., and L. L. Sloss. 1963. *Stratigraphy and sedimentation*. 2nd ed. San Francisco: Freeman and Company.
- Lee, J.-S., and J. C. Santamarina. 2005. "Bender elements: Performance and signal interpretation." *J. Geotech. Geoenviron. Eng.* 131 (9): 1063–1070. [https://doi.org/10.1061/\(ASCE\)1090-0241\(2005\)131:9\(1063\)](https://doi.org/10.1061/(ASCE)1090-0241(2005)131:9(1063)).
- Liang, K., Y. He, and G. X. Chen. 2020. "Experimental study on dynamic shear modulus and damping ratio characteristics of coral sand from Nansha Islands." [In Chinese.] *Rock Soil Mech.* 41 (1): 23–38. <https://doi.org/10.16285/j.rsm.2018.7359>.
- Liu, X., S. Li, and L. Sun. 2020. "The study of dynamic properties of carbonate sand through a laboratory database." *Bull. Eng. Geol. Environ.* 79 (7): 3843–3855. <https://doi.org/10.1007/s10064-020-01785-z>.
- Liu, X., and J. Yang. 2018. "Shear wave velocity in sand: Effect of grain shape." *Géotechnique* 68 (8): 742–748. <https://doi.org/10.1680/jgeot.17.T.011>.
- Liu, X., J. Yang, G. Wang, and L. Chen. 2016. "Small-strain shear modulus of volcanic granular soil: An experimental investigation." *Soil Dyn. Earthquake Eng.* 86 (4): 15–24. <https://doi.org/10.1016/j.soildyn.2016.04.005>.
- Lo Presti, D. C. F. 1995. "General Report: Measurement of shear deformation of geomaterials in the laboratory." In *Proc., Int. Conf. on Prefailure Deformation Characteristics of Geomaterials*, 1067–1088. Rotterdam, Netherlands: Balkema.
- Lo Presti, D. C. F., M. Jamiolkowski, O. Pallara, A. Cavallaro, and S. Pedroni. 1997. "Shear modulus and damping of soils." *Géotechnique* 47 (3): 603–617. <https://doi.org/10.1680/geot.1997.47.3.603>.
- Ma, W. J., Y. Qin, K. Zhao, and G. X. Chen. 2022. "Comparisons on liquefaction behavior of saturated coral sand and quartz sand under principal stress rotation." *Mar. Georesour. Geotechnol.* 40 (2): 235–247. <https://doi.org/10.1080/1064119X.2021.1882627>.
- Matesic, L., and M. Vucetic. 2003. "Strain-rate effects on soil secant shear modulus at small cyclic strains." *J. Geotech. Geoenviron. Eng.* 129 (6): 536–549. [https://doi.org/10.1061/\(ASCE\)1090-0241\(2003\)129:6\(536\)](https://doi.org/10.1061/(ASCE)1090-0241(2003)129:6(536)).
- Menq, F. Y. 2003. "Dynamic properties of sandy and gravelly soils." Ph.D. dissertation, Dept. of Civil Engineering, Univ. of Texas.
- Morsy, A. M., M. A. Salem, and H. H. Elmamlouk. 2019. "Evaluation of dynamic properties of calcareous sands in Egypt at small and medium shear strain ranges." *Soil Dyn. Earthquake Eng.* 116 (4): 692–708. <https://doi.org/10.1016/j.soildyn.2018.09.030>.
- Oztoprak, S., and M. D. Bolton. 2013. "Stiffness of sands through a laboratory test database." *Géotechnique* 63 (1): 54–70. <https://doi.org/10.1680/geot.10.P.078>.
- Payan, M., A. Khoshghalb, K. Senetakis, and N. Khalili. 2016. "Effect of particle shape and validity of G_{max} models for sand: A critical review and a new expression." *Comput. Geotech.* 72 (4): 28–41. <https://doi.org/10.1016/j.compgeo.2015.11.003>.
- Qadimi, A., and M. R. Coop. 2007. "The undrained cyclic behaviour of a carbonate sand." *Géotechnique* 57 (9): 739–750. <https://doi.org/10.1680/geot.2007.57.9.739>.

- Rahman, M. M., S.-C. R. Lo, and Y. F. Dafalias. 2014. "Modelling the static liquefaction of sand with low-plasticity fines." *Géotechnique* 64 (11): 881–894. <https://doi.org/10.1680/geot.14.P.079>.
- Rahmani, H., and S. A. Naeini. 2020. "Influence of non-plastic fine on static liquefaction and undrained monotonic behavior of sandy gravel." *Eng. Geol.* 275 (1): 105729. <https://doi.org/10.1016/j.enggeo.2020.105729>.
- Rollins, K. M., M. D. Evans, N. B. Diehl, and W. D. Daily III. 1998. "Shear modulus and damping relationships for gravels." *J. Geotech. Geoenviron. Eng.* 124 (5): 396–405. [https://doi.org/10.1061/\(ASCE\)1090-0241\(1998\)124:5\(396\)](https://doi.org/10.1061/(ASCE)1090-0241(1998)124:5(396)).
- Rollins, K. M., M. Singh, and J. Roy. 2020. "Simplified equations for shear-modulus degradation and damping of gravels." *J. Geotech. Geoenviron. Eng.* 146 (9): 04020076. [https://doi.org/10.1061/\(ASCE\)GT.1943-5606.0002300](https://doi.org/10.1061/(ASCE)GT.1943-5606.0002300).
- Rui, S., Z. Guo, T. Si, and Y. Li. 2020. "Effect of particle shape on the liquefaction resistance of calcareous sands." *Soil Dyn. Earthquake Eng.* 137 (2): 106302. <https://doi.org/10.1016/j.soildyn.2020.106302>.
- Salem, M., H. Elmamlouk, and S. Agaiby. 2013. "Static and cyclic behavior of North Coast calcareous sand in Egypt." *Soil Dyn. Earthquake Eng.* 55 (12): 83–91. <https://doi.org/10.1016/j.soildyn.2013.09.001>.
- Salgado, R., P. Bandini, and A. Karim. 2000. "Shear strength and stiffness of silty sand." *J. Geotech. Geoenviron. Eng.* 126 (5): 451–462. [https://doi.org/10.1061/\(ASCE\)1090-0241\(2000\)126:5\(451\)](https://doi.org/10.1061/(ASCE)1090-0241(2000)126:5(451)).
- Sandeep, C. S., S. Li, and K. Senetakis. 2021. "Experimental and analytical investigation on the normal contact behavior of natural proppant simulants." *Geomech. Geophys. Geo-Energy Geo-Resources* 7 (4): 1–15. <https://doi.org/10.1007/s40948-021-00296-9>.
- Sarkar, D., D. König, and M. Goudarzy. 2019. "The influence of particle characteristics on the index void ratios in granular materials." *Particulate* 46 (4): 1–13. <https://doi.org/10.1016/j.partic.2018.09.010>.
- Seed, H. B., and I. M. Idriss. 1970. *Soil moduli and damping factors for dynamic response analyses*. Berkeley, CA: Univ. of California.
- Seed, H. B., R. T. Wong, I. M. Idriss, and K. Tokimatsu. 1986. "Moduli and damping factors for dynamic analyses of cohesionless soils." *J. Geotech. Eng.* 112 (11): 1016–1032. [https://doi.org/10.1061/\(ASCE\)0733-9410\(1986\)112:11\(1016\)](https://doi.org/10.1061/(ASCE)0733-9410(1986)112:11(1016)).
- Senetakis, K., A. Anastasiadis, and K. Pitilakis. 2012. "Small strain shear modulus and damping ratio of quartz and volcanic sands." *Geotech. Test. J.* 35 (6): 20120073. <https://doi.org/10.1520/GTJ20120073>.
- Senetakis, K., A. Anastasiadis, and K. Pitilakis. 2013. "Normalized shear modulus reduction and damping ratio curves of quartz sand and rhyolitic crushed rock." *Soils Found.* 53 (6): 879–893. <https://doi.org/10.1016/j.sandf.2013.10.007>.
- Senetakis, K., and H. He. 2017. "Dynamic characterization of a biogenic sand with a resonant column of fixed-partly fixed boundary conditions." *Soil Dyn. Earthquake Eng.* 95 (4): 180–187. <https://doi.org/10.1016/j.soildyn.2017.01.042>.
- Sharma, S. S., and M. A. Ismail. 2006. "Monotonic and cyclic behavior of two calcareous soils of different origins." *J. Geotech. Geoenviron. Eng.* 132 (12): 1581–1591. [https://doi.org/10.1061/\(ASCE\)1090-0241\(2006\)132:12\(1581\)](https://doi.org/10.1061/(ASCE)1090-0241(2006)132:12(1581)).
- Shi, J., W. Haegeman, and T. Xu. 2020. "Effect of non-plastic fines on the anisotropic small strain stiffness of a calcareous sand." *Soil Dyn. Earthquake Eng.* 139 (2): 106381. <https://doi.org/10.1016/j.soildyn.2020.106381>.
- Thevanayagam, S. T., S. Shenthan, S. Mohan, and J. Liang. 2002. "Undrained fragility of clean sands, silty sands, and sandy silts." *J. Geotech. Geoenviron. Eng.* 128 (10): 849–859. [https://doi.org/10.1061/\(ASCE\)1090-0241\(2002\)128:10\(849\)](https://doi.org/10.1061/(ASCE)1090-0241(2002)128:10(849)).
- Wichtmann, T., M. A. Navarrete Hernández, and T. Triantafyllidis. 2015. "On the influence of a non-cohesive fines content on small strain stiffness, modulus degradation and damping of quartz sand." *Soil Dyn. Earthquake Eng.* 69 (4): 103–114. <https://doi.org/10.1016/j.soildyn.2014.10.017>.
- Wichtmann, T., and T. Triantafyllidis. 2009. "Influence of the grain-size distribution curve of quartz sand on the small strain shear modulus G_{max} ." *J. Geotech. Geoenviron. Eng.* 135 (10): 1404–1418. [https://doi.org/10.1061/\(ASCE\)GT.1943-5606.0000096](https://doi.org/10.1061/(ASCE)GT.1943-5606.0000096).
- Yamamoto, J. A., and P. V. Lade. 1997. "Static liquefaction of very loose sands." *Can. Geotech. J.* 34 (6): 905–917. <https://doi.org/10.1139/97-057>.
- Yamashita, S., T. Kawaguchi, Y. Nakata, T. Mikami, T. Fujiwara, and S. Shibuya. 2009. "Interpretation of international parallel test on the measurement of G_{max} using bender elements." *Soils Found.* 49 (4): 631–650. <https://doi.org/10.3208/sandf.49.631>.
- Yang, J., and X. Q. Gu. 2013. "Shear stiffness of granular material at small strains: Does it depend on grain size?" *Géotechnique* 63 (2): 165–179. <https://doi.org/10.1680/geot.11.P.083>.
- Yang, J., and X. Liu. 2016. "Shear wave velocity and stiffness of sand: The role of non-plastic fines." *Géotechnique* 66 (6): 500–514. <https://doi.org/10.1680/jgeot.15.P.205>.
- Yang, J., X. Liu, Y. Guo, and L. B. Liang. 2018. "A unified framework for evaluating in situ state of sand with varying fines content." *Géotechnique* 68 (2): 177–183. <https://doi.org/10.1680/jgeot.16.P.254>.
- Yang, J., and L. M. Wei. 2012. "Collapse of loose sand with the addition of fines: The role of particle shape." *Géotechnique* 62 (12): 1111–1125. <https://doi.org/10.1680/geot.11.P.062>.
- Yang, J., and X. R. Yan. 2009. "Site response to multi-directional earthquake loading: A practical procedure." *Soil Dyn. Earthquake Eng.* 29 (4): 710–721. <https://doi.org/10.1016/j.soildyn.2008.07.008>.
- Yilmaz, Y., and M. Mollamahmutoglu. 2009. "Characterization of liquefaction susceptibility of sands by means of extreme void ratios and/or void ratio range." *J. Geotech. Geoenviron. Eng.* 135 (12): 1986–1990. [https://doi.org/10.1061/\(ASCE\)GT.1943-5606.0000164](https://doi.org/10.1061/(ASCE)GT.1943-5606.0000164).
- Youd, T. L. 1973. "Factors controlling maximum and minimum densities of sands." In *Evaluation of relative density and its role in geotechnical projects involving cohesionless soils*, 98–112. West Conshohocken, PA: ASTM.
- Youn, J.-U., Y.-W. Choo, and D.-S. Kim. 2008. "Measurement of small-strain shear modulus G_{max} of dry and saturated sands by bender element, resonant column, and torsional shear tests." *Can. Geotech. J.* 45 (10): 1426–1438. <https://doi.org/10.1139/T08-069>.